Science of the Total Environment 689 (2019) 1276–1292

Contents lists available at ScienceDirect

Science of the Total Environment

journal homepage: www.elsevier.com/locate/scitotenv

Using stable isotopes paired with tritium analysis to assess thermokarst lake water balances in the Source Area of the Yellow River, northeastern Qinghai-Tibet Plateau, China

Chengwei Wan [a,b,c,d], J.J. Gibson [c,d,*], Sichen Shen [e], Yi Yi [c,f], Peng Yi [a,b,**], Zhongbo Yu [a,b]

[a] State Key Laboratory of Hydrology - Water Resources and Hydraulic Engineering, Nanjing 210098, China
[b] College of Hydrology and Water Resources, Hohai University, Nanjing 210098, China
[c] Department of Geography, University of Victoria, P.O. Box 3060, STN CSC, Victoria, BC V8W 2Y2, Canada
[d] InnoTech Alberta, 3-4476 Markham Street, Victoria, BC V8Z 7X8, Canada
[e] College of Energy and Electrical Engineering, Hohai University, Nanjing 210098, China
[f] Environmental Monitoring and Science Division, Alberta Environment and Parks, Edmonton, Alberta T5J 5C6, Canada

HIGHLIGHTS

- Stable isotopes and tritium gradients applied to assess thaw lake water balances.
- Thermokarst lake classes include ground-ice-melt and precipitation fed types.
- Thawing permafrost produced increases in water yield from catchments to lakes.
- Extensive permafrost zone had high, increasing runoff whereas others were in decline.
- Shifting hydrology due to permafrost degradation summarized in new conceptual model.

GRAPHICAL ABSTRACT

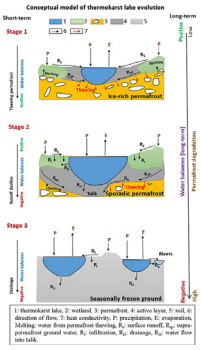

ARTICLE INFO

Article history:
Received 24 May 2019
Received in revised form 20 June 2019
Accepted 25 June 2019
Available online 30 June 2019

Editor: José Virgílio Cruz

Keywords:
Tritium
Thermokarst lake
Water balance
Isotope mass balance
Permafrost degradation
Hydrological changes

ABSTRACT

A spatially distributed network of thermokarst lakes undergoing significant environmental changes was sampled in 2014 and 2016 to develop a comprehensive understanding of lake water balances in lakes across a gradient of frozen ground conditions. Frozen ground ranges from seasonally frozen ground (SFG) to sporadic discontinuous permafrost (SDP) to extensive discontinuous permafrost (EDP), and is representative of complex conditions in the Source Area of the Yellow River, northeastern part of Qinghai-Tibet Plateau. Radioactive and stable water isotopes in reference lakes (non-thaw lakes), thermokarst lakes, precipitation, wetlands, ground ice and supra-permafrost groundwater are analyzed to characterize systematic variations and to assess lake water balances using stable isotope mass balance (IMB). IMB, paired with analysis of tritium decay gradients, is shown to be a valid approach for detecting short-term shifts in lake water balance, which allows evaluation of the proportion of precipitation-derived versus permafrost-derived water inputs to lakes. All lakes except EDP thaw lakes are evaporation-dominated ($E/I > 0.5$). Negative water balances occurred most frequently in reference lakes due to hydrological connectivity with rivers. Precipitation-derived water inputs result in positive water balances in SFG and SDP thermokarst lakes, but negative-trending water balances are found in SDP thermokarst lakes due to substantial reduction in water yield. Increasing contributions from thawing permafrost in EDP thermokarst

* Corresponding author at: Department of Geography, University of Victoria, P.O. Box 3060, STN CSC, Victoria, BC V8W 2Y2, Canada.
** Corresponding author at: State Key Laboratory of Hydrology - Water Resources and Hydraulic Engineering, Nanjing 210098, China.
E-mail addresses: jjgibson@uvic.ca (J.J. Gibson), pengyi1915@163.com (P. Yi).

https://doi.org/10.1016/j.scitotenv.2019.06.427

lakes result in strong positive water balance. Permafrost degradation may also lead to the changes in hydrological connectivity between precipitation and wetlands or thermokarst lakes. Based on these findings, a conceptual model of the hydrological evolution of thermokarst lakes under the influence of permafrost degradation is proposed.

1. Introduction

Climate change has been widely implicated as the major cause of rapid permafrost degradation in arctic and subarctic regions of the northern hemisphere and Qinghai-Tibet plateau (QTP) as revealed by numerous recent studies (Hinzman et al., 2005; Cheng and Wu, 2007; Jin et al., 2009; Yang et al., 2010; Liljedahl et al., 2016; Ran et al., 2017). Thermokarst lakes (also known as thaw lakes) are a common landscape feature in these regions, forming as a result of thawing of locally ice-rich permafrost or melting of massive ground ice. The occurrence of thermokarst lakes is signal of permafrost degradation and often indicates unstable and warming permafrost conditions (Yoshikawa and Hinzman, 2003). The deepening and expansion of small, shallow ponds and/or lakes and increasing thermokarst intensity have been widely reported over the last decade in areas such as Central Yakutia, Alaskan Arctic Coastal Plain, Yukon and southern QTP (continuous permafrost). Latent heat storage in newly formed water bodies frequently becomes the dominant heat source in winter, leading to further acceleration of thawing, subsidence and formation of water-rich depressions (Arp et al., 2011; Lin et al., 2010, 2011; Niu et al., 2011; Boike et al., 2016; Roy-Leveillee and Burn, 2017; Ulrich et al., 2017). Progressive permafrost degradation may also result in increased active layer depths, slumping or erosion of drainage channels, formation of taliks below lakes, increased interaction with sub-permafrost groundwater, and eventually may result in shrinkage, drainage, or disappearance of thermokarst lakes (Yoshikawa and Hinzman, 2003; Smith, 2005; Lantz and Turner, 2015). Ulrich et al. (2017) suggested that evolution of thermokarst lakes is often complicated by several factors including permafrost zonation, geomorphology of the catchment, and reshaping of the surface and subsurface thermal regimes, which can lead to changes in lake sizes and numbers, as confirmed by Macdonald et al. (2016).

Thermokarst lakes are an important water resource and have significant hydrological, ecological, and biogeochemical roles in cold regions systems (Niu et al., 2011; Kokelj and Jorgenson, 2013; Heslop et al., 2016). The hydrological behavior of thermokarst lakes can strongly affect regional water mass balance, intensify thermokarst processes, alter water quality, increase mobilization of contaminants, and release fresh organic carbon, thereby accelerating carbon cycling and greenhouse gas production (Kokelj et al., 2005; MacDonald et al., 2012; Anthony et al., 2014; Bond and Carr, 2018). Shifts in water balance processes triggered by climate change have also been suggested as a potential driver of thermokarst lake evolution (Gibson et al., 2015; Chen et al., 2014; Narancic et al., 2017; Pan et al., 2017; Gao et al., 2018).

While there are thousands of thermokarst lakes distributed across QTP undergoing significant climatic and hydrological changes, the quantitative mechanisms driving these processes are not yet fully understood. Due to the lack of long-term hydrometeorological monitoring and large-scale investigations, previous studies mainly focused on thermokarst lakes in small- or mesoscale basins including several well-known large lakes. Emphasis has been placed on characterization of changes in the numbers or areas of lakes, qualifying the contributions of permafrost-derived meltwater to thaw lakes, and estimation of evaporation-to-inflow or precipitation-to-inflow ratios, although these studies have not succeeded in quantifying the major hydrological fluxes (Lin et al., 2010, 2011; Pan et al., 2014, 2017; Luo et al., 2014a, 2014b, 2018a, 2018b, 2018c, 2018d; Yang et al., 2016, 2019; Gao et al., 2018). Recent studies have documented that direct precipitation on lake surfaces was a minor source of inflow to thermokarst lakes compared to inflow from the lake drainage basin including surface and subsurface recharge and permafrost thaw sources, which dominated the water balance (Yang et al., 2016, 2017; Pan et al., 2017; Gao et al., 2018). To our knowledge, Yi et al. (2018a) first calculated the runoff depths of very limited numbers of thermokarst lake catchments in the Yellow River source region. Although this study confirmed variations in runoff (or water yield) across different permafrost landscapes, it did not attempt to rank hydrological vulnerability of these landscapes, nor did it establish the corresponding water balance conditions for lakes. While great diversity of lake water balances has been found in lake-focused case studies carried out at sites within the QTP, there is still a recognized gap in understanding the broader relationship between permafrost gradients, permafrost degradation, and the corresponding hydrological responses of thermokarst lakes (Yi et al., 2018a, 2018b, 2018c; Yang et al., 2019).

Situated in the southeastern part of the QTP, the Source Area of the Yellow River (SAYR) is characterized by a mosaic of different frozen ground types including seasonally frozen ground (SFG), sporadic discontinuous permafrost (SDP, permafrost coverage: 0–10%), extensive discontinuous permafrost (EDP, permafrost coverage: 10–50%) and continuous permafrost (permafrost coverage: >90%). Note that the permafrost classifications used here are based on the standards proposed by the International Permafrost Association (Lewkowicz et al. (2011); Bond and Carr (2018)). As such, the SAYR provides an ideal district to evaluate a range of hydrological regimes across a gradient of frozen ground conditions, as well as providing the opportunity to assess thermokarst processes across a broad continuum of lake water balance conditions. Yi et al. (2018b) previously reported that supply of the subsurface inflows to a small thermokarst lake in the EDP area accounted for between approximately 30 and 60% of the total volume of this lake. This finding indicated that hydraulic exchange between groundwater and thermokarst lakes may be more significant than for rivers, as the average proportion of groundwater recharge to rivers has been shown to be smaller than 20% in this region (Zheng et al., 2016). Yi et al. (2018a, 2018c) also provided multiple lines of isotopic evidence to confirm that thermokarst lakes likely receive more water input than other lakes.

The isotope mass balance (IMB) approach utilizing oxygen-18 (^{18}O) and deuterium (^{2}H) contained within the water molecule ($^{1}H^{1}H^{18}O$, $^{1}H^{2}H^{16}O$) has been recognized as an effective method for assessment of lake water budgets, providing valuable quantitative information on evaporation loss and water residence time. In many high-latitude regions as well as in some permafrost areas within the QTP, IMB methods have provided detailed characterization of lake hydrological fluxes (Gibson and Edwards, 2002; Macdonald et al., 2016; Narancic et al., 2017; Yang et al., 2017, 2019; Gao et al., 2018). Furthermore, based on the approach summarized by Gibson et al., 2016a, water yield estimates based on the IMB method have been shown to be particularly useful in ungauged basins for quantifying and comparing runoff responses across wide-area surveys of lakes in complex wetland-rich terrain (Gibson et al., 2015, 2016c, 2017, 2018, 2019; Yang et al., 2016; Narancic et al., 2017). While informative, regional IMB models based on stable isotopes do not generally allow for separation of the proportions of hydrological components in lake inflow, although tritium has been shown to be informative for this purpose in past studies.

Tritium (^{3}H), with a half-life of 12.32 years, is a naturally occurring radioactive isotope of hydrogen, that was introduced into the atmosphere in large quantities during atmospheric weapons testing in the late 1950s and early 1960s. Unlike other solute tracers such as ^{14}C or ^{32}Si, tritium activities are quite stable and not impacted by geochemical or biological reactions (Cartwright and Morgenstern, 2016, 2018). Tritium movement in permafrost is mainly dependent on temperature-induced mass transport instead of molecular diffusion (Burn and Michel, 1988).

While relatively few studies have measured tritium concentrations in water bodies located in permafrost terrain (Gibson et al., 2016b; Yi et al., 2018a; Bond and Carr, 2018), these studies have consistently reported higher tritium concentrations in thermokarst lakes compared to other surface water bodies, evidently implying enhanced input from thawing of modern (post 1950s) permafrost. While informative, none of these studies have endeavored to measure or compare tritium concentrations directly in permafrost or ground ice, nor did they characterize or apply a tritium decay gradient approach as demonstrated to be informative for inflow source identification by Samalavičius and Mokrik (2016) and Yi et al. (2018a).

The major aims of this paper are 1) to describe stable isotope and tritium variations in thermokarst lakes across a gradient of permafrost conditions in the SAYR; 2) to apply the IMB and tritium decay gradient methods, and to combine these approaches to characterize both water balance and sources of input to thermokarst lakes; 3) to characterize systematic shifts in hydrology across the permafrost gradient and in response to ongoing permafrost degradation, and 4) to summarize current understanding of hydrological processes in a newly developed conceptual model applicable to the wide range of permafrost conditions observed in the SAYR and beyond. Our main hypothesis is that the IMB method, paired with tritium analysis, will provide a sharper focus on underlying causes of hydrological changes as compared to using IMB alone, which was similarly noted by Bond and Carr (2018). Specifically, we hypothesize that measurement of tritium decay gradients may be a robust, complimentary indicator of short-term water balance shifts in water bodies affected by permafrost and frozen ground.

2. Study area

The study region is located in the northeastern part of Qinghai-Tibet Plateau between 95°55′ to 98°41′E and 33°56′ to 35°31′ N, an area of 2.9 × 10^4 km^2 which defines the headwater catchment or Source Area of the Yellow River (SAYR; Jin et al., 2009; Luo et al., 2011; Fig. 1). The area is flanked by mountain ranges on three sides; by the Buqing Mountains in the north, Geshigeya Mountains in the west, and the Bayan Har Mountains in the south; which together form the watershed divide. Elevation ranges from a low of 4200 m a.s.l in the eastern valley near the watershed outlet at Duoshixia, to 5267 m a.s.l at the peak of the Bayan Har Mountains (Luo et al., 2018c).

The Yellow River originates from the west and flows eastward, augmented by a drainage network of numerous mountainous tributaries and small creeks that collect to fortify flow in the main channel. In addition, thousands of lakes are widely distributed across the SAYR. Total surface area of lakes is approximately 1665 km^2 or 8% of the SAYR, and includes two large lakes, Gyaring and Ngoring Lakes (ELH and

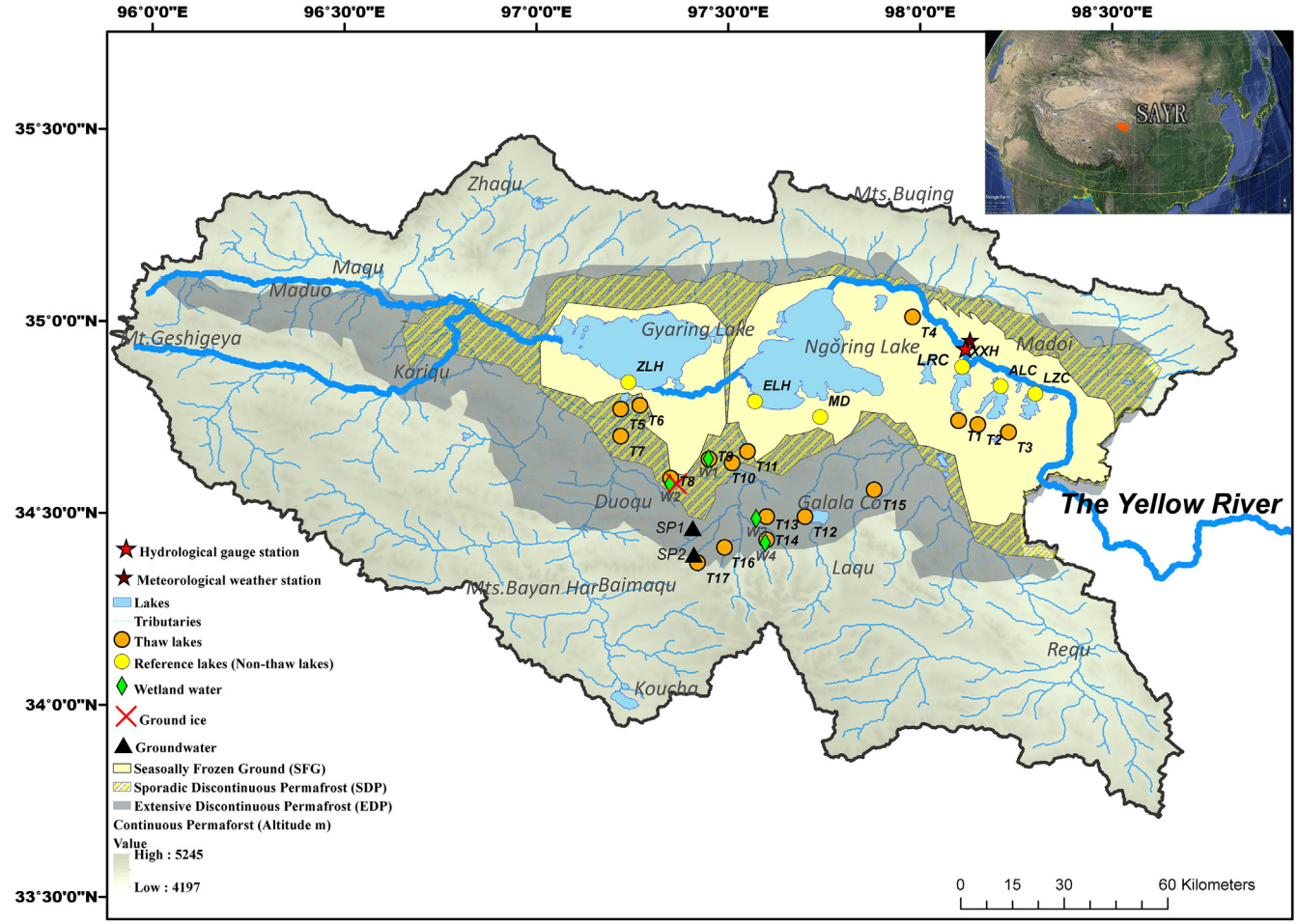

Fig. 1. Map of the Source Area of the Yellow River (SAYR), showing locations of sampling sites, water bodies and permafrost characteristics of the region.

ZLH) which are throughflow lakes of the Yellow River, and a cluster of four other prominent lakes situated near Madoi Town (Xingxinghai: XXH, Ayongwama Co: ALC, Ayonggama Co: LZC and Longre Co: LRC; shown in Fig. 1).

The climate of the region can be classified as continental, semi-arid alpine (Li et al., 2016). Based on the only long-term climate record in the region (Madoi Town; 98°13′E, 34°55′N, 4272 m a.s.l; Fig. 1), the warmest month is normally July (7.8 °C) and the coldest month is January (−16.1 °C), as recorded over the 1956–2014 period. More recent short-term climate observations have also revealed a wide range in annual air temperature and annual precipitation across the region. Site-specific field studies across the region by Luo et al. (2014a, 2014b, 2018d) reported mean annual air temperatures ranging from +4.7 °C to −5.0 °C, and mean annual precipitation ranging from 311 to 501 mm, typically with 30 rain days and 80 snow days per year. Rainfall in the warm season (April–October) accounts for 80% of total precipitation amount. The annual evaporation capacity of open water can exceed 1300 mm, and the annual average actual evapotranspiration from the land surface is estimated at around 300 mm. Most rivers and lakes freeze up from November to April (Yi et al., 2018b).

A variety of complicating factors such as elevation, topography, hydrogeology and local climate zoning, as well as presence of open water bodies influences the distribution of seasonally and perennially frozen soil. Generally, frozen ground occurs as a mosaic of different zone types including seasonally frozen ground (SFG), sporadic discontinuous permafrost (SDP), extensive plateau discontinuous permafrost (EDP) and continuous permafrost (Jin et al., 2009; Luo et al., 2018c; Wang et al., 2018a). Permafrost in the SAYR is warm (>–2.0 °C), thin (<100 m), ice-rich (high ice content near permafrost table) and thermally unstable, and so is considered to be vulnerable to climate warming (Li et al., 2016; Luo et al., 2018d). Permafrost thickness varies between 2 and 80 m depending on permafrost types and conditions, while active layer thicknesses vary between 0.6 and 3.0 m, resulting from spatial differences in thermal regimes in the presence of vegetation and peaty substrates (Luo et al., 2014a, 2014b, 2018b). The permafrost in the source area of the Yellow River is mainly elevation-dependent, with a vertical lapse rate of about 4 °C/km on the north slopes of the Bayan Har Mountains (Luo et al., 2018c). High ground ice content of deposits in plains and platforms, and the collapse of ice mounds and pingos caused by permafrost degradation since the 1970s, promote the development of thermokarst pits and ponds as well as taliks (Jin et al., 2009). Three representative zones were established to characterize conditions over gradients in the substrate, frozen soil types, and extent of permafrost degradation in SFG, SDP, and EDP, each zone based on a range of watersheds with numerous lakes (Fig. 2), as described below.

Zone 1 (Madoi) is mainly covered by SFG (coverage > 90%) in dry lands, whereas sporadic and plateau discontinuous permafrost under wetlands occurs only at the boundary between Zone 1 and Zone 3, where elevation increases above 4350 m. Previous surveys have shown that permafrost underlying soils in Madoi town had completely disappeared during the 1970 to 1990 period, with an increase in seasonally frozen ground and taliks from thawed permafrost near the four lakes cluster (Jin et al., 2009). Bare-soil desert is one notable landscape in Zone 1. Importantly, the groundwater table in this zone was found to be regionally declining, with a drop of 2 m occurring during 1980–2000 (Jin et al., 2009). The relationship between lakes, rivers and groundwater could be reversed once the ground table is lowered below the surface water levels, resulting in reduction of surface water resources (Cheng and Jin, 2013).

Zone 2 (TCM) is located on fluvial fan underlain with SDP, and at the northern and southern zone edges is interspersed with SFG and EDP, respectively, which has resulted in various landscapes from sandy land, alpine grassland to dense paludal meadows. Thermokarst lakes grow numerous and wide-ranging in TCM due to the acceleration of degrading ice-rich permafrost, approaching 60% by weight. Prominent features include thawed and collapsed pingos and palsas, dried thermokarst ponds, and widespread wetlands (mainly bogs) associated with patches of continuous and discontinuous permafrost (Jin et al., 2009).

Zone 3 (CLP) is a region with well-developed EDP, with the smallest active layer thickness and thickest depth of permafrost (Luo et al., 2018c). Peaty organic matter of up to 0.5 m occurs above the permafrost table, holding high soil moisture content and promoting dense and stable vegetation (Luo et al., 2018d). Many small creeks and thaw ponds receive overland flow from melting of massive ground ice, which is typically exposed at the soil surface due to retrogressive thaw slumping, as

Fig. 2. Representative thermokarst lakes and permafrost-related landscapes.

noted during field observations in spring and summer seasons (Luo et al., 2018a, 2018b, 2018c, 2018d; Yi et al., 2018a).

3. Materials and methods

3.1. Field sampling and analysis

Field investigations were carried out in 2014 and 2016 within the study region, including sampling of seasonally frozen ground (Zone 1, SFG), sporadic discontinuous permafrost (Zone 2, SDP), and extensive discontinuous permafrost (Zone 3, EDP). In this study, large lakes (>200 ha) are designated as reference lakes due to the fact that they are not presently under the direct influence of permafrost degradation, as no permafrost has been reported near lakeshores or beneath the lake bottoms for these lakes since the 1970s (Yi et al., 2018a). In contrast, thermokarst lakes were found to be under the direct influence of permafrost, occurring in areas of ground subsidence related to permafrost thawing, and fed by permafrost-derived meltwater. In Zone 1 (SFG), many thermokarst lakes continue to persist following complete loss of permafrost, and so may only receive water input contributions from non-permafrost sources.

Water samples for both stable isotopes and tritium were collected during both visits to the sites during 16 April to 6 May 2014 and 12 May to 21 May 2016 (Fig. 1). In total, there were 14 samples from 7 reference lakes, 34 samples from 17 thermokarst lakes of different sizes, and 8 samples from wetlands situated near 4 selected thermokarst lakes (see Table 1). Lake waters were sampled at 1-m depth near the lake centre. Opportunistically, during the sampling program, four samples of precipitation were gathered to assist with defining the local meteoric water line (LWML). To determine the isotopic compositions of permafrost-related groundwater, and for better understanding of the influence of permafrost thawing on the water cycle, 4 samples of supra-permafrost groundwater (i.e. from above the permafrost table) were extracted from two boreholes drilled in late spring in 2014 and 2016 when the thaw depth approached the full active layer depth at these sites in Zone 3. Five ground ice samples were also taken from one 3.5-m ice core collected in Zone 2.

Liquid water samples were stored in 500 ml high-density polyethylene bottles without any headspace and tightly sealed to minimize evaporation. Stable isotope and tritium samples were stored at 4 °C until returned to the lab at which time the lid seals were checked again and samples were then held at room temperature until analyzed. All ice samples were kept frozen after sampling and then melted for the first time at room temperature in sealed bottles prior to analysis.

Tritium concentration measurements were completed by using a low-activity liquid scintillation counting spectrometer (LSC, Tri–Carb 3170 TR/SL) with three counting cycles and a 120 min count time for each cycle. Tritium concentrations are reported in tritium units (T.U) with analytical uncertainty estimated at <0.3 T.U. The samples collected in 2014 were measured in August 2014, and the samples collected in 2016 were measured in June 2016. These tritium values, together with all historic tritium data discussed in this paper, were corrected for radioactive decay by normalizing to a common datum (20th May 2016). The collected water samples were analyzed for δ^2H and $\delta^{18}O$ using a Thermo Scientific Delta V Advantage Dual Inlet/HDevice system at the InnoTech Alberta lab located in Victoria, Canada. Results are expressed in δ notation in per mil (‰) relative to Vienna Standard Mean Ocean Water (V-SMOW) and normalized on the VSMOW/SLAP scale (Standard Light Arctic Precipitation). Analytical uncertainty is better than 0.1‰ for $\delta^{18}O$ and 1‰ for δ^2H, respectively.

3.2. Development of tritium decay gradients

Tritium gradient analysis has proven to be an effective method to identify recharge-discharge patterns of water bodies (Yi et al., 2018a).

The tritium decay gradient (TDG) represents the observed change in tritium concentration measured in a specific water body during a fixed time period, which is defined as:

$$\mathrm{TDG} = \frac{N_i - N}{T}$$

where N_i is the initial tritium concentration of a specific water body (T.U), N is the measured tritium concentration (T.U) of the same water body after time T, T is the time interval (yr).

Also, a theoretical tritium decay gradient (TG) is defined as:

$$\mathrm{TG} = \frac{N_i - N_r}{T}$$

$$N_r = N_i \times e^{-T/17.93}$$

where N_i is the initial measured tritium concentration (T.U), N_r is the residual tritium concentration (T.U) after radioactive decay time, T (yr).

The theoretical tritium gradient represents a gradient corresponding exactly to the theoretical rate of tritium decay, so therefore is always positive (>0). If the TDG/TG ratio > 1 then we can conclude that the lake may be recharged by water sources with mean tritium concentrations lower than the lake water. Conversely, if the TDG/TG ratio < 1 we can conclude that the input water to the lake may contain mean tritium concentrations that are higher than the lake water.

3.3. Estimating water mass balance using stable isotopes

A reference plot in $\delta^{18}O$-δ^2H space (Fig. 5) was developed to illustrate and compare lake water samples to precipitation, wetlands, groundwater, ground ice and the Local Meteoric Water Line (LMWL) based on Ren et al. (2013). Lakes are shown to plot along a linear trend close to predicted Local Evaporation Lines, which were calculated for each zone based on the linear resistance model of Craig and Gordon (1965) under the assumption that the isotope composition of atmospheric moisture (δ_A) was in equilibrium with the isotope composition of amount-weighted average annual precipitation (δ_P) at prevailing local atmospheric conditions (i.e. temperature (T) and relative humidity (h)), and the evaporation-flux weighted method used to modify T and h values as recommended by Gibson et al. (2016a). The isotope mass balance (IMB) methodology, as applied in previous studies of thermokarst and non-thermokarst lakes (Gibson et al., 2016c; Narancic et al., 2017; Gao et al., 2018), was then applied to describe site-specific hydrology of lakes.

We used the lake water isotope compositions (δ_L) measured in 2014 and 2016 in each lake to calculate evaporation-to-inflow (E/I) ratios for each year under the assumption that lakes were well-mixed (common for shallow lakes) and that isotopic composition of inflow can be approximated by the isotopic composition of precipitation (i.e. $\delta_P = \delta_I$). Evaporation-to-inflow is given by:

$$E/I\ (or\ x) = (\delta_I - \delta_L)/(\delta_E - \delta_L) \quad (1)$$

where δ_E is the isotopic composition of evaporated water (Gibson et al., 2016a):

$$\delta_E = ((\delta_L - \varepsilon^+)/\alpha^+ - h\delta_A - \varepsilon_K)/\left(1 - h + 10^{-3}\varepsilon_K\right) \quad (2)$$

ε^+ is the equilibrium isotopic separation (Horita and Wesolowski, 1994), α^+ is the equilibrium isotopic fractionation (i.e. $\varepsilon^+ = \alpha^+ - 1$), ε_K is the kinetic isotopic separation (Horita et al., 2008), and δ_A is the isotopic composition of atmospheric moisture:

$$\delta_A = (\delta_P - \varepsilon^+)/\alpha^+ \quad (3)$$

Table 1
Isotopic data for samples from different water bodies in this study, including stable oxygen and hydrogen isotopes, tritium concentrations, tritium decay gradients and theoretical gradients. Tritium values are decay corrected to May 20th 2016.

Water body ID	Type of sample	Sampling time	Longitude	Latitude	Elevation (masl)	Stable isotopes			Tritium concentration		Tritium decay gradient (T.U year^{-1})	Theory gradient (T.U year^{-1})
						$\delta^{18}O$ (‰ V-SMOW)	$\delta^{2}H$ (‰ V-SMOW)	D-excess	Bq/L	T.U		
MADOI, zone 1; seasonally frozen ground												
P1	Precipitation	2014/4/19	98°07′54″	34°56′20″	4215	−9.5	−67.1	9.0	0.71	6.3		
		2016/5/20				−11.9	−85.2	10.0	0.71	6.3		
P2	Snow	2014/4/19	98°07′54″	34°56′20″	4215	−7.8	−61.1	1.7	0.98	8.7		
		2016/5/20				−9.9	−69.8	9.2	0.90	8.0		
T1	Thermokarst lake	2014/4/15	98°05′49″	34°44′12″	4215	−0.7	−21.5	−16.1	1.69	15.0	1.21	0.89
		2016/5/17				−1.0	−22.2	−13.9	1.61	14.3		
T2	Thermokarst lake	2014/4/16	98°09′09″	34°43′49″	4260	0.8	−22.8	−29.2	1.81	16.1	1.15	0.95
		2016/5/18				−0.5	−24.2	−20.1	1.77	15.7		
T3	Thermokarst lake	2014/4/16	98°13′34″	34°42′42″	4230	−1.4	−26.3	−15.5	1.86	16.5	1.48	0.98
		2016/5/18				−2.9	−36.3	−13.2	1.74	15.5		
T4	Thermokarst lake	2014/4/16	97°58′50″	35°00′21″	4245	−1.5	−32.0	−19.8	1.82	16.2	1.24	0.96
		2016/5/18				−2.0	−32.2	−15.9	1.76	15.6		
XXH	Reference lake (non-thaw)	2014/4/14	98°06′35″	34°52′31″	4118	2.3	1.1	−17.6	1.36	12.1	1.20	0.72
		2016/5/11				1.3	−2.6	−13.0	1.25	11.1		
ALC	Reference lake (non-thaw)	2014/4/16	98°12′22″	34°49′57″	4143	0.3	−14.6	−17.1	1.34	11.9	1.32	0.71
		2016/5/11				0.2	−15.5	−16.9	1.20	10.6		
LZC	Reference lake (non-thaw)	2014/4/26	98°17′43″	34°48′53″	4200	0.2	−15.9	−17.5	1.32	11.8	1.50	0.70
		2016/5/18				0.1	−16.1	−16.8	1.14	10.1		
TCM, zone 2; sporadic discontinuous permafrost												
T5	Thermokarst lake	2014/4/18	97°13′23″	34°46′16″	4278	−4.3	−44.8	−10.4	2.30	20.4	2.79	1.21
		2016/5/20				−2.9	−33.6	−10.4	1.93	17.1		
T6	Thermokarst lake	2014/4/19	97°16′04″	34°46′56″	4274	−4.5	−45.2	−9.5	2.10	18.6	2.44	1.09
		2016/5/20				−2.9	−34.6	−11.6	1.82	16.2		
T7	Thermokarst lake	2014/4/20	97°13′20″	34°41′47″	4285	−3.7	−36.5	−7.0	1.78	15.8	1.13	0.93
		2016/5/20				−3.5	−37.2	−8.9	1.73	15.4		
T8	Thermokarst lake	2014/4/26	97°21′06″	34°35′31″	4296	−3.1	−35.8	−10.9	1.96	17.4	1.16	1.03
		2016/5/21				−4.1	−44.5	−11.9	1.93	17.1		
T9	Thermokarst lake	2014/4/26	97°26′59″	34°38′29″	4346	−2.1	−27.6	−11.0	1.93	17.1	0.97	1.01
		2016/5/21				−2.7	−34.6	−13.4	1.94	17.2		
T10	Thermokarst lake	2014/4/26	97°30′21″	34°38′05″	4282	−4.7	−51.9	−14.5	1.85	16.4	1.55	0.97
		2016/5/21				−4.3	−49.7	−15.0	1.71	15.2		
T11	Thermokarst lake	2014/4/26	97°32′45″	34°39′20″	4285	−4.4	−45.9	−10.8	1.77	15.7	1.90	0.93
		2016/5/21				−4.0	−48.7	−16.9	1.54	13.7		
ELH	Reference lake (non-thaw)	2014/4/19	97°34′21″	34°47′10″	4285	0.8	−12.5	−19.0	1.40	12.4	1.46	0.74
		2016/5/20				0.5	−14.3	−18.1	1.23	10.9		
ZLH	Reference lake (non-thaw)	2014/7/24	97°14′28″	34°50′25″	4364	0.2	−18.6	−19.9	1.40	12.4	1.64	0.73
		2016/5/21				−0.3	−18.3	−16.1	1.21	10.7		
MD	Reference lake (non-thaw)	2014/4/16	97°44′20″	34°44′56″	4284	0.5	−11.2	−15.6	1.65	14.7	1.19	0.87
		2016/5/15				0.4	−13.6	−16.7	1.58	14.0		
W1	Wetland	2014/4/17	97°26′55″	34°38′28″	4422	1.3	−6.5	−16.9	1.90	16.9	0.91	1.00
		2016/5/17				1.6	−7.1	−19.8	1.92	17.1		
W2	Wetland	2014/4/26	97°20′52″	34°34′34″	4567	1.7	−6.6	−20.0	1.90	16.8	0.97	1.00
		2016/5/21				1.6	−7.0	−19.6	1.90	16.9		
G1	Ground ice	2016/5/19	97°13′31″	34°35′22″	4456	−13.2	−91.5	13.8	2.16	19.2		
G2	Ground ice	2016/5/19				−14.0	−97.2	15.1	2.21	19.6		

(continued on next page)

Table 1 (*continued*)

Water body ID	Type of sample	Sampling time	Longitude	Latitude	Elevation (masl)	Stable isotopes			Tritium concentration		Tritium decay gradient (T.U year^{-1})	Theory gradient (T.U year^{-1})
						δ^{18}O (‰ V-SMOW)	δ^{2}H (‰ V-SMOW)	D-excess	Bq/L	T.U		
G3	Ground ice	2016/5/19				−14.3	−98.2	16.3	2.34	20.8		
G4	Ground ice	2016/5/19				−14.5	−99.4	16.9	2.47	21.9		
G5	Ground ice	2016/5/19				−13.7	−94.8	14.9	2.75	24.4		
CLP, zone 3; extensive discontinuous permafrost												
T12	Thermokarst lake	2014/4/16	97°41′53″	34°29′34″	4414	−8.8	−74.9	−4.6	2.15	19.1	0.76	1.13
		2016/5/19				−9.1	−71.7	0.9	2.24	19.9		
T13	Thermokarst lake	2014/4/22	97°35′50″	34°29′10″	4548	−9.3	−80.7	−6.3	2.05	18.2	0.64	1.07
		2016/5/21				−10.1	−81.6	−0.8	2.15	19.1		
T14	Thermokarst lake	2014/4/23	97°36′10″	34°25′55″	4634	−9.0	−69.6	2.2	2.27	20.1	0.83	1.19
		2016/5/18				−9.4	−72.9	2.3	2.35	20.9		
T15	Thermokarst lake	2014/4/18	97°52′37″	34°33′20″	4604	−8.9	−70.2	1.0	2.31	20.6	1.05	1.22
		2016/5/19				−9.0	−72.6	−0.3	2.35	20.9		
T16	Thermokarst lake	2014/4/23	97°29′08″	34°24′50″	4633	−8.9	−71.6	−0.1	2.27	20.1	1.01	1.19
		2016/5/18				−9.1	−75.0	−1.8	2.31	20.5		
T17	Thermokarst lake	2014/4/18	97°25′05″	34°21′59″	4600	−6.9	−56.7	−1.5	2.28	20.3	1.01	1.20
		2016/5/19				−7.2	−63.4	−5.8	2.33	20.7		
SP1	Groundwater	2014/4/15	97°24′28″	34°27′38″	4515	−12.9	−92.2	11.3	1.64	14.5	0.38	0.86
		2016/5/17				−12.3	−88.7	9.6	1.75	15.5		
SP2	Groundwater	2014/4/17	97°24′38″	34°37′30″	4625	−12.4	−90.9	8.2	1.14	10.2	0.58	0.60
		2016/5/19				−11.9	−83.9	11.1	1.15	10.2		
W3	Wetland	2014/4/18	97°33′22″	34°28′06″		1.3	−7.7	−18.4	2.12	18.9	0.53	1.12
		2016/5/19				1.5	−8.5	−20.6	2.26	20.1		
W4	Wetland	2014/4/18	97°35′47″	34°29′21″	4611	0.8	−10.6	−16.8	2.34	20.8	0.67	1.23
		2016/5/20				1.5	−7.1	−18.8	2.12	18.8		

Considering that:

$$I = P + R \tag{4}$$

where P is the precipitation falling directly on the lake surface and R is the ungauged total flow from the watershed, we can estimate R based on:

$$R = E/x - P\ (\mathrm{m3 \cdot yr}) \tag{5}$$

given that Evaporation is known or can be estimated. Given that $x = E/I$, $E = e \cdot LA$ and $P = p \cdot LA$; e and p are the annual depth of evaporation and precipitation ($\mathrm{m \cdot yr^{-1}}$), and LA is the lake area ($\mathrm{m^2}$), water yield (WY) can be estimated as:

$$WY = R/DBA \cdot 1000\ (\mathrm{mm \cdot yr^{-1}}) \tag{6}$$

where DBA is the drainage basin area of individual lake ($\mathrm{m^2}$), $DBA = WA - LA$, and WA is the watershed area of individual lake ($\mathrm{m^2}$). Runoff ratio can be defined as WA ($\mathrm{mm \cdot yr^{-1}}$) / p ($\mathrm{mm \cdot yr^{-1}}$), also expressed as R/P.

Mean annual estimates of δ^{18}O and δ^{2}H in precipitation (δ_{P}) are amount-weighted values based on the amount and isotopic composition of 175 individual precipitation events sampled during 2009–2010 from Ren et al. (2013). Climatic parameters in 2014 and 2016 including mean annual air temperature, annual total precipitation and mean monthly relative humidity in the three different zones were derived from China National Meteorological Information Center (http://cdc.Cma.Gov.cn/home.do). Actual evaporation rates of open water in each zone based on daily field observations during the study period were corrected to estimate the accumulated actual evaporation depths (e) during the open water season (Jin et al., 2009). Lake surface areas (LA) are extracted from Surface reflectance Tier 1 products of Landsat L8-OLI-based 30-m resolution imagery in 2014 summer, where scenes are selected with low cloud and shadow coverage (<5%) by Google Earth Engine (GEE, https://code.earthengine.google.com/dataset/LANDSAT/LC08/C01/T1_SR). A non-parametric, unsupervised method using adaptive threshold detection integrated with MNDWI, Canny Edge Filter, and Otsu Thresholding, is applied to help auto-extract the LA for each lake in GEE. Details of the methodology and programming codes can be found in Donchyts et al. (2016). Watershed areas (WA) were calculated for each sampling site in the ArcGIS program using the ArcHydro tools based on 30-m digital elevation model (DEM) data, where each watershed was delineated upstream of a lake outlet. High-resolution Google Earth images and 1:250000 geological and environmental maps compiled for the SAYR during 2001 to 2004 were also used to confirm the delineated results of each watershed. The summary of surface areas and watershed areas are shown in Table 2.

Table 2
The morphometry summary of lakes and lake watersheds.

Morphometry	Other lakes	Thaw lakes		
		SFG	SDP	EDP
Surface area ($\mathrm{km^2}$)	211.8 ± 266.5	2.15 ± 0.76	0.05 ± 0.11	3.7 ± 8.3
Drainage basin area ($\mathrm{km^2}$)	915.5 ± 1095.2	11.4 ± 3.3	0.4 ± 0.6	27.1 ± 59.3
Shape	Round	Elliptical	Elliptical	Elongated

4. Results

4.1. Tritium activities

Tritium concentrations are highly variable among the sampled water bodies, as summarized in box plots in Fig. 3. The lowest tritium activities were found in present-day precipitation, with mean values of 7.3 T.U, ranging from 6.3 to 8.7 T.U., and confirmed to be significantly distinct from other groups based on K-W ANOVA test $H_3 = 62.5$, $p < 0.001$). Ground ice was found to contain the highest average tritium concentration of 21.2 ± 1.9 T.U, and is distinct from most other groups (K-W ANOVA, $H_3 = 26.5$, $p < 0.001$), with the exception of wetland water and thermokarst lakes. Wetland water was found to range from 16.8 to 22.0 T.U, with a mean value of 18.3 ± 1.5 T.U. For thermokarst lakes, average tritium concentration was 17.9 ± 2.4 T.U compared with 11.9 ± 1.3 T.U in reference lakes. A K-W ANOVA test shows that wetlands, thermokarst lakes and reference lakes are all statistically different (K-W ANOVA, $H_3 = 31.4$, $p < 0.001$). Reference lakes are not found to be significantly different than groundwater based on the Mann-Whitney *U* test ($U = 23$, $n_1 = 12$, $n_2 = 4$, $p = 0.952$).

Highest tritium concentrations were found in EDP thermokarst lakes (20.4 ± 0.6 T.U), while tritium concentrations were generally lower and more variable in SDP thermokarst lakes (17.1 ± 2.0 T.U). SFG thermokarst lakes were found to have the lowest tritium values (15.6 ± 0.7 T.U). Among the frozen ground zones, tritium content in thermokarst lakes clearly shows a progressive increase from SFG to SDP to EDP as permafrost presence and prevalence increases.

Tritium values for wetland water in Zone 2 was found to be 16.9 ± 0.1 T.U whereas in Zone 3 it was 20.4 ± 1.3 T.U., differences found to be statistically significant. In contrast, thermokarst lakes in both Zones 2 and Zone 3 did not have significantly different tritium values than local wetland water as suggested by Mann-Whitney tests ($p = 0.749$ and $p = 0.952$, respectively). While tritium content in ground ice evidently differed from wetland water in Zone 2 (Mann-Whitney, $U = 20$, $n_1 = 5$, $n_2 = 4$, $p < 0.01$), it is not statistically different from wetland water in Zone 3 ($p = 0.806$).

The tritium content of local precipitation and groundwater during the 1980–1990 period, a period when permafrost degradation was expected to have begun or when it significantly accelerated, are also shown in Fig. 3. Tritium in current groundwater is statistically indistinguishable from both the historic precipitation and the supra-permafrost water sampled in 1980–1990, indicating the persistence of 1980–1990 water in the subsurface. Note that peak tritium concentrations in the atmosphere in SAYR was almost 2000 T.U in 1963 which, if corrected for radioactive decay to 2016, corresponds to a comparatively high value of ~103 T.U. A positive correlation ($r^2 = 0.98$, $N = 5$) is found between the depth-below-surface and tritium concentrations of ground ice, implying that samples of ground ice in this study likely originated from historic precipitation recharged between approximately 1963 and 1980 as noted by Yi et al. (2018a).

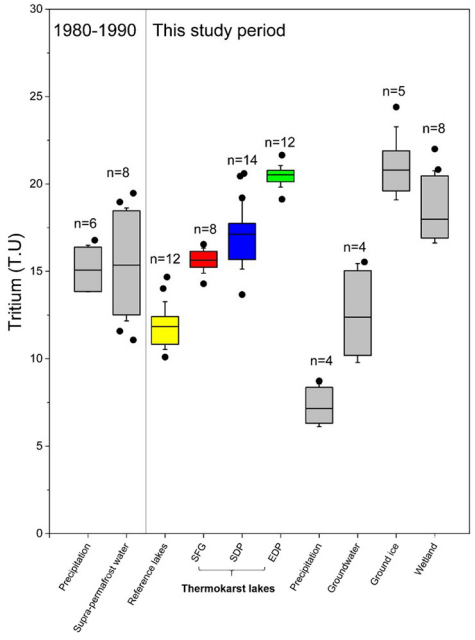

Fig. 3. Box plot showing tritium concentrations in different water bodies measured during this study (right), compared to historical records (Yi et al., 2018a). Note that all tritium values are decay-corrected to 20th May 2016 to permit direct comparisons.

4.2. Tritium decay gradients

Comparison of observed tritium decay gradients and theoretical decay gradients in different water bodies are useful for examining recharge or discharge patterns (Fig. 4), as described below. As expected, precipitation samples fall close to the 1:1 line (TDG = TG), which reflects that tritium activity in the atmosphere is dominated by radioactive decay. As tritium in modern precipitation is found to be <10 T.U, it appears that atmospheric tritium concentrations are returning to natural background (pre-1950) levels. The reference lakes, together with all SFG and SDP thermokarst lakes (with the exception of T9 lake) fall above the 1:1 line, indicating that input to these lakes is dominated by tritium-depleted sources. In contrast, EDP thermokarst lakes and wetland water, as well as groundwater, plot below the 1:1 line, which implies that sources supplying the water bodies contain relatively higher tritium concentrations.

It is notable that wetland water has relatively lower TDG/TG ratios compared with lake water in each zone. TDG/TG ratios of wetlands are found to be spatially variable, with values of 0.94 ± 0.04 T.U·yr^{-1} for Zone 2 and 0.51 ± 0.05 T.U·yr^{-1} for Zone 3, respectively. It can be inferred that wetlands in Zones 2 and 3 may have different recharge-discharge patterns.

4.3. Stable isotope framework

Stable isotope analyses are plotted in $\delta^{18}O$–$\delta^{2}H$ space to illustrate labelling of the various water sources relative to the LMWL

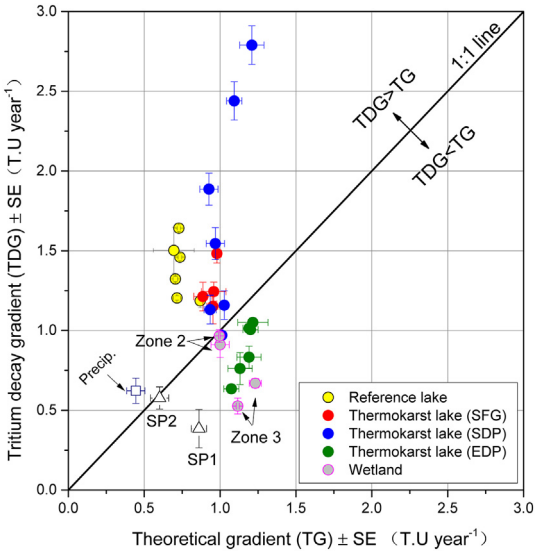

Fig. 4. Tritium decay gradients (TDG) versus theoretical gradients (TG) including standard error bars for different water bodies. Note that water bodies that fall above the 1:1 line are likely fed by water sources with lower tritium concentrations, while water bodies that fall below the 1:1 line are likely mixed with waters of higher tritium concentrations. Higher TG means higher tritium concentrations in water bodies in 2014.

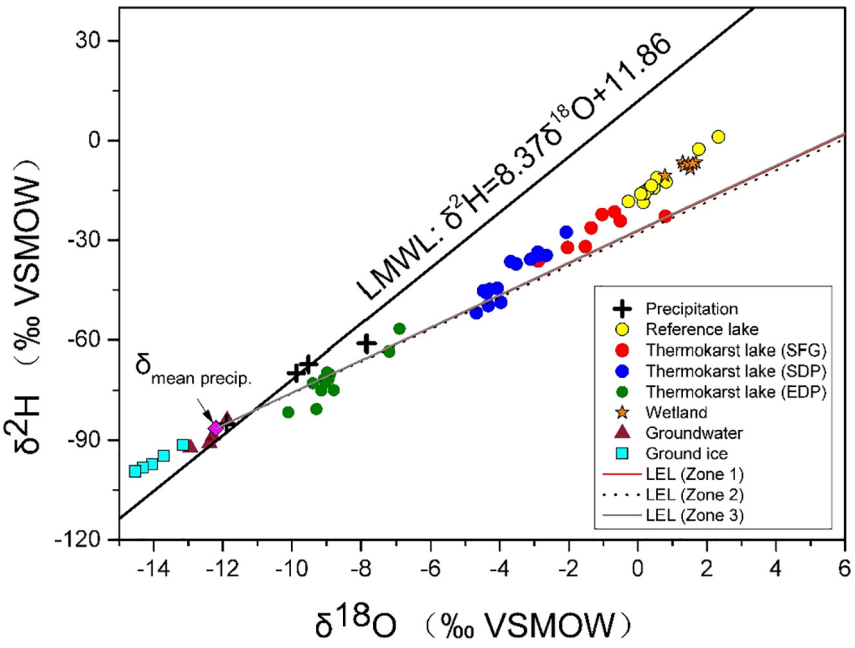

Fig. 5. Isotopic compositions of water samples plotting on a δ^2H versus $\delta^{18}O$ diagram. Note that the pink diamond indicates the amount-weighted rainfall isotope value (−12.2‰ for $\delta^{18}O$, −86.4‰ for δ^2H). The three predicted Local Evaporation Lines (LELs) are calculated from data shown in Table 3. (For interpretation of the references to colour in this figure legend, the reader is referred to the web version of this article.)

and evaporative enrichment of lakes from the various zones (Fig. 5). The isotope composition of reference lakes and thermokarst lakes in the three zones are found to be clustered, suggesting similarity of water balances within each group. Higher offset from the LMWL is noted for reference lakes indicating more evaporative water balances, with systematically reduced offset, and hence lower evaporation losses in successive categories from SFG to SDP to EDP.

Parameters used to plot predicted LELs (Table 3) utilized gridded FW *T* and FW *h* data (2-year means) as well as a constant value for δ_P based on Ren et al. (2013). The similarity between predicted LELs for all zones reflects similarity in climate. While the predicted LELs closely match the slope of the observed evaporative enrichment in SDP and EDP lakes, reference lakes (and to some extent SFG lakes) appear to fall slightly above the predicted trends, which may indicate that the lakes are evaporating at slightly higher humidity due to evaporative feedback from the lakes to the local atmosphere (see Jasechko et al., 2014). In particular, this situation is enhanced by the large size of many of the reference lakes. Lack of permafrost in reference and SFG lakes may also lead to enhanced subsurface infiltration and reduced runoff of snowmelt, potentially biasing inputs to non-permafrost lakes in favor of more enriched summer precipitation values. Enriched input values could also be influential in steeper evaporation slopes.

The isotopic compositions of supra-permafrost groundwater (mean: −12.4‰ for $\delta^{18}O$ and −88.9‰ for δ^2H) are close to δ_P, which confirms that active-layer storage can be approximated as an average mixture of recent precipitation. While no samples of deep groundwater from sub-permafrost or non-permafrost areas were collected to assess if they may be more snowmelt rich, this effect has been widely observed in areas of Canada with seasonally frozen soils (Carey and Pomeroy, 2009). Unlike the groundwater and other water sources, ground ice is characterized by the most depleted compositions (Mean: −14.0‰ for $\delta^{18}O$ and −96.2‰ for δ^2H) and low variability ($\delta^{18}O$: −14.5 to −13.2‰, δ^2H: −99.4 to −91.5‰). Ground ice clusters above the LMWL, with a regression line given by $\delta^2H = 5.8\delta^{18}O - 15.2$, which is consistent with deep-buried ground ice originating from sub-modern precipitation rather than modern water (Yang et al., 2017, 2019).

4.4. Modelling outputs of lake water mass balance

Lake-specific ratios of E/I, P/I and lake catchment-specific water yields (WY) and runoff ratios (R/P) are calculated for both 2014 and 2016 based on the methodology presented in Section 3.3. Results confirm and quantify the striking differences observed for specific lakes and lake classes (Fig. 6). The E/I and P/I ratios are shown in all cases to have negative correlations with tritium concentrations, while positive

Table 3
Derived and calculated parameters used to develop the isotope mass balance (IMB) model.

Parameter	Zone 1		Zone 2		Zone 3	
	2014	2016	2014	2016	2014	2016
FW T (K)	273.94	274.34	273.92	274.32	271.94	272.34
FW h	0.527	0.527	0.561	0.561	0.561	0.561
α^+ (^{18}O, ^2H)	1.0117, 1.111	1.0117, 1.112	1.0117, 1.111	1.0117, 1.110	1.0120, 1.114	1.0120, 1.113
ε^+ (^{18}O, ^2H)	0.0117, 0.111	0.0117, 0.112	0.0117, 0.111	0.0117, 0.110	0.0120, 0.114	0.0120, 0.113
ε_K (^{18}O, ^2H)	6.81, 6.00	6.81, 6.01	6.23, 5.49	6.23, 5.49	6.23, 5.49	6.23, 5.49
δp (^{18}O, ^2H) ‰	−12.2, −86.4	−12.2, −86.4	−12.2, −86.4	−12.2, −86.4	−12.2, −86.4	−12.2, −86.4
δ_A (^{18}O, ^2H) ‰	−23.6, −178.5	−23.6, −176.9	−23.7, −177.4	−23.6, −176.9	−23.9, −179.2	−23.8, −179.2

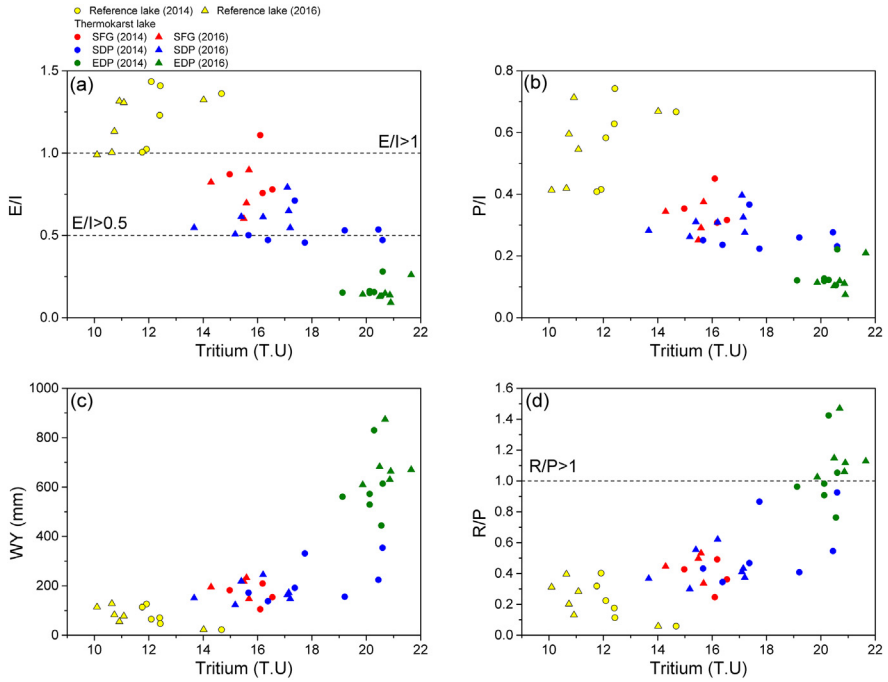

Fig. 6. IMB derived water balance indicators for thermokarst lakes (SFG, SDP, EDP) and reference lakes, including: (a) evaporation-to-inflow (E/I) ratios, (b) precipitation-to-inflow (P/I) ratios (c) annual water yield, and (d) runoff ratios. Note that E/I and P/I reflect water balance conditions in the lakes whereas water yield and runoff ratios reflect conditions in the respective lake catchments.

correlations are found for water yield and runoff ratios, all statistically significant at $p < 0.001$.

4.4.1. Evaporation-to-inflow ratios (E/I) and precipitation-to-inflow ratios (P/I)

For reference lakes, it is apparent that water losses by evaporation exceeded liquid outflows for the two years sampled, with predominantly higher E/I ratios than other lake categories (Table 4). E/I values were found in most cases to be higher than 1, suggesting also that the lakes had little leakage and may have been actively reducing in volume due to evaporation. This situation can be regarded as a strongly negative water balance. E/I ratios for SFG thermokarst lakes were somewhat less enriched, in the range of 0.60 to 1.11, which again indicates an evaporative (or negative) water balance although some lakes are also losing significant amounts of water to liquid outflow. For SDP thermokarst lakes, E/I ratios are found to be comparatively lower, averaging 0.57 with a narrow range straddling the boundary between negative and positive water balances (0.46 to 0.79). In contrast, EDP thermokarst lakes were found to have the lowest E/I ratios, with a mean value of 0.16 and ranging between 0.09 and 0.28 (Table 4), implying consistently positive water balance.

Differences in E/I ratios were also estimated based on 2014 and 2016 surveys and applied to assess positive or negative trends over this interval (Table 4). With the exception of SDP thermokarst lakes, the majority of lake classes (and individual lakes) were found to have decreasing E/I ratios indicating positive shifts in water balance. Change in E/I (ΔE/I) for reference lakes, SFG and EDP thermokarst lakes ranged from −1.5 to −30.8% (and were generally more pronounced in SFG lakes) confirming a trend to more positive water balances for these systems. For SDP, ΔE/I ranged from +1.5 to +30.8%, indicating more evaporative negative-trending water balance conditions. Interestingly, nearly 60% of thermokarst lakes in the SDP area had negative water balances (i.e. E/I > 0.5) whereas in 2016 this number had increased to 100%.

P/I ratios reflect the fraction of total inputs by precipitation on lake surfaces, and are therefore expected to be sensitive to factors such as lake area, catchment area and permafrost extent, the latter expected to govern conditions such as hillslope water availability, evapotranspiration, infiltration, and runoff amounts. P/I for all reference lakes, overall the largest lakes surveyed, is estimated to be >0.5 (or 50%), whereas thermokarst lakes are found to be entirely below this threshold. In general, EDP lakes have the lowest P/I values (between 0.07 and 0.22), presumably due to relatively large influxes of lateral inflows from these permafrost-rich catchments, and systematically increase as permafrost extent diminishes. For SDP lakes we note P/I values in the range of 0.22 to 0.40, and for SFG, 0.25 to 0.45.

General trends in P/I between 2014 and 2016 (Table 4) follow the same pattern found for E/I, and are attributed mainly to increased precipitation in the latter year. For SDP lakes, consistent positive trends in both E/I and P/I are more strongly linked to reduced input, presumably due to reduction in catchment water sources.

4.4.2. Water yield (WY) and runoff ratio (R/P)

Water yield from EDP thermokarst lake catchments is shown to range from 400 to 900 mm/year (Fig. 6c), significantly higher than any other group, with consistently higher runoff ratios (0.76 to 1.47). Average water yield of EDP lakes (640 mm/yr) is roughly 3 times higher than both SDP lakes and SFG lakes, which were similar (200 mm/yr versus 181 mm/yr), and >8 times higher than water yield to reference lakes (77 mm/yr). Mean runoff ratios displayed similar gradients, ranging from >1.0 for EDP lakes, 0.4 to 0.6 for SDP or SFG lakes, and <0.2 for reference lakes. Catchment water contributions are clearly enhanced in areas with increased permafrost coverage.

From 2014 to 2016, water yield increased by nearly 20% in half of the reference lake catchments, with concomitant changes noted in runoff ratios, while the remainder underwent only slight increases in water yield and runoff ratio (<3%). For thermokarst lakes there were substantial increases noted in water yield and runoff ratio, both in SFG and EDP thermokarst lakes. In contrast, SDP lakes underwent reduction in water yield and runoff ratio, reflecting unique evolutionary water balance trajectories for the different hydrological regimes.

Table 4
Calculated components of the water budget of lakes and hydrological features of drainage basins in 2014 and 2016.

		Reference lake			Thermokarst lake							
					SFG			SDP			EDP		
		2014	2016	Δ(%)	2014	2016	Δ(%)	2014	2016	Δ(%)	2014	2016	Δ(%)
Climate factors	T (°C)	−2.84 to −2.5	−2.74 to −2.4	+3.5–4%	−2.5	−2.4	+4	−2.84	−2.74	+3.5	−4.8	−4.2	+12.5
	P (mm)	404.9 ± 16.1	416.9 ± 6.6	+3	426.4	438.4	+2.8	390.8 ± 8.0	402.8 ± 8.2	+3.1	582	594.8	+2.2
	E (mm)	915.7	925.6	+1.1	1050.1	1078.5	+2.7	789	816.2	+3.4	738.7	750.5	+1.6
Lake water balance parameters	I (mm)	761 ± 202	797 ± 194	+4.7	1222 ± 172	1424 ± 222	+16.5	1533 ± 189	1319 ± 171	−13.9	4546 ± 903	5367 ± 1506	+18.1
	E/I	1.24 ± 0.17	1.18 ± 0.14	−5.2	0.88 ± 0.14	0.76 ± 0.11	−14.1	0.53 ± 0.08	0.61 ± 0.09	+16.1	0.17 ± 0.05	0.15 ± 0.05	−12.2
	P/I	0.57 ± 0.12	0.56 ± 0.11	−2.5	0.36 ± 0.06	0.32 ± 0.05	−11.7	0.26 ± 0.05	0.31 ± 0.04	+17.2	0.14 ± 0.04	0.12 ± 0.04	−10.3
Watershed hydrological conditions	WY (mm)	74 ± 36	80 ± 35	+8.3	163 ± 39	199 ± 32	+22.1	224 ± 80	175 ± 39	−22.0	591 ± 119	689 ± 87	+16.4
	R/P	0.18 ± 0.08	0.19 ± 0.08	+5.4	0.38 ± 0.09	0.45 ± 0.07	+18.8	0.57 ± 0.21	0.44 ± 0.10	−23.2	1.01 ± 0.20	1.16 ± 0.15	+14.1

5. Discussion

5.1. Isotope hydrology of thermokarst lakes and source waters

A clear pattern of isotopic enrichment emerges from our analysis of lakes in different permafrost zones in the SAYR. Stable isotopic composition of lakes ($\delta^{18}O$ and $\delta^{2}H$) is found to be controlled mainly by evaporative enrichment under similar atmospheric conditions but different water balance conditions at each site. Water balance is found to be closely related to or determined by the extent of permafrost in the various zones, and results in systematic groupings of lakes in $\delta^{18}O$-$\delta^{2}H$ space (Fig. 5). Progressive isotopic enrichment is generally found along the following gradient:

EDP<SDP<SFG<reference

which corresponds to a general decline in the extent and influence of permafrost.

Tritium concentrations in lake water are similarly systematic, although tritium gradients are reversed, with higher tritium concentrations being correlated with greater permafrost extent, as follows:

Reference<SFG<SDP<EDP

Anti-correlation between tritium and stable isotopes is confirmation that tritium concentrations are not controlled by evaporation, but likely by the proportion of modern (post-1950s) permafrost thaw sources, as noted by Gibson et al. (2016b) for sites in Canada.

Stable isotope enrichment in lakes closely follows the predicted LEL trajectory in $\delta^{18}O$-$\delta^{2}H$ space for EDP and SDP lakes, but SFG and reference lakes fall slightly above this trend which is perhaps related to moisture buildup over the lakes, and/or bias in snowmelt recharge in permafrost-free areas. While previous studies have cautioned that the LMWL and LEL intercept may yield biased estimates of inflow sources (see Benettin et al., 2018), we find reasonable agreement between the intercept and measured isotopic composition of precipitation.

Based on both the IMB assessments and tritium gradient analyses, two main input sources to lakes are established, namely precipitation, which may fall directly on the lake surface or on the catchment, the latter contributing in turn to surface or subsurface water yield, and permafrost-related water, including supra-permafrost water and ground ice, which also contribute to increases in the water yield. While these sources are often indistinctly labelled by stable isotopes (Gibson et al., 2015; Narancic et al., 2017), indirect evidence from E/I, P/I, WY, and R/P calculations for both 2014 and 2016 (Fig. 6) have helped to understand the spatial and temporal gradients in these sources. As tritium content in lake water generally falls in the range between rainfall (with the lowest value of 6.3 T.U) and ground ice (with the highest value of 24.4 T.U) (Fig. 3), partitioning of these sources can also be evaluated. Importantly, a positive correlation between tritium concentration and permafrost extent directly emphasizes that the proportion of thawing permafrost contributing to inflow is progressively increased from Zone 1 to Zone 3 (Luo et al., 2018a, 2018b, 2018c).

From assessment of TDG/TG ratios (Fig. 4), it is also apparent that better definition of input sources can be achieved from analysis of temporal tritium gradients. Because there is no existing ground ice in Zone 1, which contains both reference and SFG lakes, the current inflow contribution to these lakes from permafrost is negligible, and the major input is precipitation. In most cases these lakes have TDG/TG > 1 indicating recent addition of sources depleted in tritium relative to lake waters. Persistence of high tritium values in these lakes relative to modern precipitation sources is attributed mainly to storage of old water, these lakes being large lakes (>1 km^2) with depths reaching >3 m, and which are therefore expected to have residence times of many years. For SFG thermokarst lakes in Zone 1, it is important to note that permafrost was present (mainly as ground ice) up until the late 1970s (Jin

et al., 2009; Yi et al., 2018a). A previous study demonstrated that SFG thermokarst lakes operated as hydrologically closed-systems, and that they have high $^{129}I/^{127}I$, which is attributed to past permafrost thaw (Yi et al., 2018c). Reference lakes receive replenishment of rivers and release great amounts of water to the downstream, which is also confirmed by the enriched $^{129}I/^{127}I$ and stable isotope ratios in the nearby lakes and rivers (Yi et al., 2018a, 2018c). Slightly higher ranges of TDG/TG for reference lakes relative to SFG lakes may indicate that a component of water contributions from tritium-free sources, perhaps glacial melt or deep groundwater, in the former.

High tritium found among SDP and EDP thermokarst lakes and ground ice directly reflects their formation from thawing permafrost. Particularly, tritium concentrations in ground ice are more enriched than thermokarst lakes, groundwater and wetland water, with lower TDG/TG ratios (<1) suggestive of higher proportions of permafrost meltwater relative to other sources. Previously, subsurface water has been shown to account for between about 30 and 60% of source water in a typical EDP thermokarst lake (Yi et al., 2018b). Supra-permafrost groundwater that was sampled at depths of 0.6 m (SP1) and 0.2 m (SP2) below ground surface in the EDP area, were found to have mean tritium concentrations of 15.0 and 10.2 T.U., respectively. SP1 displays a lower TDG/TG ratio, similar to wetland water (W3, W4) in Zone 3 (Fig. 4). $\delta^{18}O$ and $\delta^{2}H$ signatures of SP1 are very close to the average isotopic composition of ground ice. Meanwhile, no differences are noted in stable isotope signatures or TDG/TG between SP2 and precipitation, which suggests that active layer water near the ground surface may contain precipitation, but that it may not infiltrate into deeper soils. By comparison, deeper soil water close to the permafrost table is expected to be comprised mainly of ground ice melt.

Lower elevation areas of Zone 2 and Zone 3 contain wetlands originating from thawed and collapsed pingos (Jin et al., 2009). Similar wetland water was sampled within the SDP (W1, W2) and EDP areas (W3, W4), and within thermokarst lake catchments (T9, T8, T13, T14), and was found to be relatively enriched in stable isotopes, revealing high levels of evaporation loss and sluggish flow. A range of tritium concentrations and TDG/TG in wetland waters indicate different hydrologic responses in Zone 2 and Zone 3. Note that tritium concentrations in wetlands are slightly reduced compared to thermokarst lakes, and, along with similarity of TG/TDG between wetlands (0.97, 0.91) and near-surface groundwater (0.96), suggest that water sources are precipitation dominated rather than being derived from permafrost thaw sources. The presence of 1980–1990 supra-permafrost water in Zone 2 wetlands suggests a significant storage of old water and low mobility of water in the perennial wetland, such that it is effectively sustained for long periods under evaporative conditions (Yi et al., 2018a). While the tritium concentration of wetland water in Zone 3 are generally higher than thermokarst lakes but lower than ground ice in the same drainage basin, it appears that wetland water may have been derived from ground ice melt, and then subsequently released to thermokarst lakes as noted by Gibson et al. (2016b). These findings emphasize that wetlands may form early in the permafrost thaw process prior to the formation of thermokarst ponds (Wang et al., 2018b). Gradually deepening seasonal thaw depths tend to melt and finally exhaust ground ice, changing the landscape and increasing subsurface storage. The supply-discharge relationships between wetlands and thermokarst lakes may reverse as the reduction of permafrost coverage induces groundwater table lowering, which changes conditions for the recharge and discharge (Cheng and Jin, 2013). As a result, drainage of lakes may occur via hydraulic pathways created from lateral erosion of soils and/or due to vertical taliks in the latter stages. While isotopes may assist to better understand the relationship between permafrost thaw, ground ice formation, and wetland and thermokarst lake development, complete understanding of these processes requires further study.

5.2. Temporal shifts from 2014 to 2016

In 2016, E/I for SFG lakes and reference lakes was 2 to 23% lower than estimated in 2014 (Table 4). Although air temperature dramatically increased, the measured evaporation loss fraction declined as slightly higher evaporation rates were more than compensated for by increased precipitation and runoff. Reference lakes, together with SFG and SDP lakes, are classified as evaporation-dominated lakes due to annual losses exceeding 50% of total inflow by volume (Turner et al., 2010; Gao et al., 2018). Reference lakes are more extreme examples of evaporative lakes as they appear to be systems experiencing drawdown given that E > I for 2014 and 2016 surveys. On average, direct precipitation accounts for 57% and 34%, respectively, of the total inflows for reference lakes and SFG thermokarst lakes. Importantly, their hydrological behavior is in general contrast to other large lakes studied in southern QTP such as Tangra Yumco and Nam Co, which show positive water balance due to recently increased precipitation (Biskop et al., 2016; Kang et al., 2017).

The two biggest lakes sampled in this survey (ELH and ZLH) are headwater flow lakes which serve as reservoirs to regulate the annual discharge of the Yellow River (Fig. 1). An 18 to 19% increase in water yield to these lakes suggests that more runoff was being generated upstream of the lakes in 2016 compared to 2014, but the total input by runoff and precipitation on the lake is still less than the sum of water losses via evaporation and downstream outflow (Table 4). Note that P/I of the two lakes is over 60%, which means the precipitation on lake surfaces is the most important influence on this process. Reference lakes ALC and LZC (Fig. 1) are found to be close to the E = I balance point in 2014 and 2016, with $P/I < 50\%$. Field investigations suggest that these lakes were hydrologically disconnected from the Yellow River and tributaries in 2014/16 in contrast to other reference lakes such as XXH and MD where $E/I > 1.3$ and $P/I > 0.5$, which are known to recharge to river when water levels increased in response to intensive summer rainfall (Yi et al., 2018a). Similarly, most SFG thermokarst lakes show slightly positive water balance ($E/I < 1$) due to no interaction with rivers, and they appear in many cases to accumulate precipitation-related runoff from their watershed instead of depending on direct precipitation on lake surface ($P/I < 0.5$). Comparison of water balance between SFG lakes and reference lakes with no connection to rivers (ALC, LZC) reveals more similar runoff responses.

5.3. Spatial and temporal indicators

Use of both spatial and temporal water balance indicators has been shown here to be informative for study of thermokarst lakes in the SAYR as it has been for lake districts in many other parts of the world. Previous studies and reviews have discussed the uncertainties related to IMB and have generally concluded that the method, while ideally suited for assessment of site-to-site variability in lake water balance, is not preferred as a stand-alone approach without supportive physical monitoring for a single site or watershed (Gibson et al., 2016a). Nevertheless, the value of the method for obtaining the general features of the regional water balance and for characterizing variability in ungauged systems in this study is indisputable. Yet it is interesting to ask if we might have gained similar insight from a one-time stable isotope survey conducted in either year.

IMB results based on either 2014 or 2016 would have established a spatial trajectory of shifting ratios of E/I, P/I, WY and R/P (y-axis, Fig. 6) which can be recognized among individual lakes and between the various lake groups. These indicators illustrate many of the key water balance processes across the region, and already serve as a basis for better understanding of the system. Tritium surveys based on either 2014 or 2016 (y-axis, Fig. 6) would likewise have provided confirmation that high WY thermokarst systems (also characterized by high R/P, low E/I and low P/I) have anomalously high tritium, which, given water sources in the present setting, may only be attributed to melting of

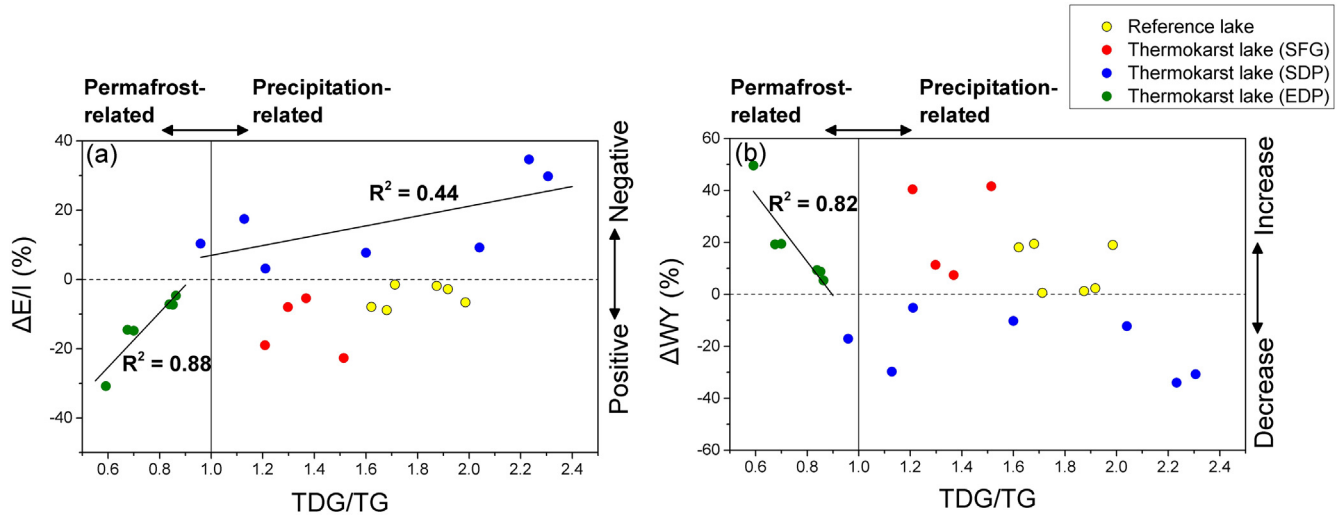

Fig. 7. Relationships between IMB water balance indicators and the ratios of actual tritium decay gradient to theoretical decay gradient (TDG/TG) for thermokarst lakes (SFG, SDP, EDP) and reference lakes, including: (a) change in evaporation-to-inflow ratios (ΔE/I) between 2014 and 2016 (%); and (b) change in annual water yield (ΔWY) between 2014 and 2016 (%).Note that ΔE/I reflects changes in lake water balance whereas ΔWY reflects changes in runoff from the respective lake catchments.

permafrost containing significant bomb tritium. Repeat sampling in 2014 and 2016 provides additional confidence in the results, but what additional information has temporal sampling provided?

In the case of SAYR, short-term changes in lake water balances between 2014 and 2016 are likely representative of the systematic and widespread hydrological shifts that have occurred due to a warming and wetting climate across the region (Table 4). Correlations between temporal shifts in both stable isotopes and tritium (e.g. ΔE/I, ΔWY versus TDG/TG, Fig. 7a, b) establish a useful framework for visualization and classification of both positive and negative shifts in water balance, information on the underlying cause of shifts, namely permafrost thaw versus precipitation-related changes (Fig. 7a), as well as increasing versus decreasing runoff (Fig. 7b). For EDP lakes, robust correlations between ΔE/I versus TDG/TG ($r^2 = 0.88$, Fig. 7a) and ΔWY versus TDG/TG ($r^2 = 0.82$, Fig. 7b) capture systematic positive shifts due mainly to permafrost-related changes. For SDP lakes, the strength of transition to more negative water balances appears to be due to decreasing runoff (Fig. 7b) but is significantly dependent on the degree of influence from permafrost thaw sources, as revealed again by a correlation between ΔE/I versus TDG/TG ($r^2 = 0.44$, Fig. 7b). Post-melt systems such as SFG and reference lakes are shown to be undergoing positive shifts in water balance mainly driven by precipitation-related changes, and cluster by group indicating similarity, but do not display clear trends likely due to weaker drivers (see Fig. 7a,b).

Overall, from the combined assessment of spatial thermokarst lake patterns and analysis of short-term temporal shifts, a clearer picture of thermokarst lake development emerges for the SAYR. Early in the permafrost degradation cycle, meltwater enhances runoff and produces more positive water balances in newly formed thermokarst lakes. As melt proceeds, runoff gradually declines as permafrost sources become depleted, the active layer deepens and taliks reduce the connectivity of the lakes and their watersheds. At the present time, melting in extensive discontinuous permafrost (EDP) watersheds continues to generate >8 times higher runoff (WY) than reference lakes and WY was found to increase by 50 mm/year on average between 2014 and 2016. In contrast, sporadic discontinuous permafrost (SDP) watersheds produced 2.5 times higher runoff (WY) than reference lakes, but were found to be decreasing on average by 25 mm/year during 2014 to 2106. Progressive permafrost thaw appears to produce a pulse of meltwater analogous to an event hydrograph, with both a rising limb and falling limb. While the duration of the pulse is expected to vary depending on specific regional conditions, observations in the SAYR suggest that this pulse will conclude within several decades.

5.4. Conceptual model of thermokarst lake development

Evolutionary changes in lake and wetland coverage across the QTP and SAYR has been attributed to different stages of permafrost degradation (Li et al., 2008; Mao et al., 2018). Consistently for SAYR, both wetland areas and lake areas have varied significantly over the past 30 years due to increasing melt-related disturbances in water balance including changes in water supply, runoff, drainage and overall annual budgets. Across the region, the majority of small ponds and lakes, together with swamps and wetlands, increased during 2004–2012 (Tong et al., 2014). Based on the enrichment of tritium signatures in these systems, and positive shifts inferred for lake water balances under the permafrost-increased gradients, we consider that reverse shifts in hydrological regimes could be representative of sustained permafrost disturbances. Based on this premise, a conceptual model of hydrological variability and change of thermokarst lakes under 3 stages of progressively degrading permafrost conditions is developed as follows (Fig. 8):

Stage 1: in ice-rich permafrost, as shallow permafrost begins to thaw due to changes in surface heat balance, local subsidence occurs due to melting of both intergranular and massive ground ice. Meltwater released into the active layer enhances moisture availability, leads to development of wetlands, and enhances local runoff to lakes contributing to additional erosion, deepening, and volumetric enlargement of lakes. Consequently, thermokarst lakes show strongly positive water balances and experience lateral expansion as a result of higher water yields from melting ground ice and high runoff ratios. Some studies have also reported runoff enhancement due to enhanced connectivity, leading also to increase in precipitation-related runoff (overland and subsurface flows) as well as an increase in meltwater from the thawing upper-permafrost (Ala-Aho et al., 2018a, 2018b; Zheng et al., 2018).

Stage 2: as permafrost degradation continues, ground ice is consumed and eventually will become exhausted. Deepening of the active layer and reduction in ice-content leads to decline in thaw sources to wetlands and thermokarst lakes, although thermokarst lakes may continue to grow and modify the thermal characteristics of the surrounding landscape including the formation of taliks (Fedorov et al., 2014; Selroos et al., 2019). Enhanced infiltration and vertical connectivity in unfrozen

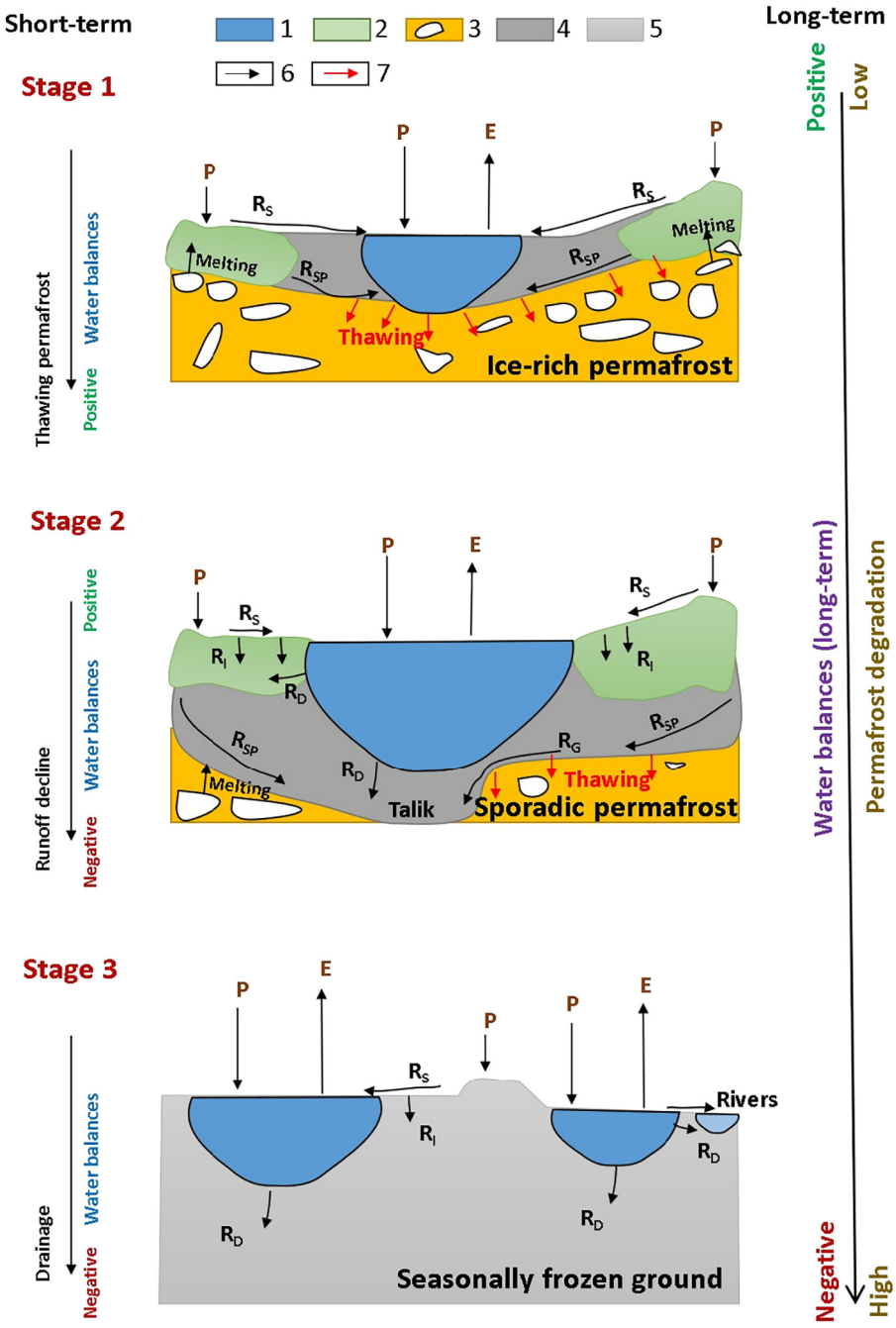

Fig. 8. Conceptual model illustrating the evolution of thermokarst lakes under processes of permafrost degradation. 1: thermokarst lake, 2: wetland, 3: permafrost, 4: active layer, 5: soil, 6: direction of flow, 7: heat conductivity, P: precipitation, E: evaporation, melting: water from permafrost thawing, R_s: surface runoff, R_{sp}: supra-permafrost ground water, R_I: infiltration, R_D: drainage, R_C: water flow into talik.

soils is expected to occur as permafrost becomes less pervasive and no longer serves as an effective aquitard (Cheng and Jin, 2013; Yang et al., 2019). Consequently, sporadic discontinuous permafrost (SDP) thermokarst lakes are formed, which receive reduced quantities of runoff, lower runoff ratios and may potentially develop sub-permafrost groundwater connections including lake drainage. Others have noted that enhanced drainage of thermokarst lakes, either laterally or vertically, can produce a feedback effect on the permafrost degradation (Ma et al., 2017). In stage 2, thermokarst lakes become more evaporation-dominated due to the significant reduction in water yield.

Stage 3: as the perennially frozen system turns into a seasonally frozen one, permafrost meltwater ceases, evaporation becomes more dominant, and seasonally frozen ground (SFG) thermokarst lakes are established. Such lakes are now entirely reliant on precipitation or groundwater sources for replenishment although seasonal frost may still be influential in determining the timing of runoff. In Stage 3, thermokarst lakes are likely to undergo areal and water level decline, they may divide into multiple water bodies, or complexly drain. In some cases, thermokarst lakes are sustained by interaction with rivers, connections which may have been enhanced by the thermal/mechanical erosion process. Such lakes are representative of reference lakes used in this study, and can be considered to be mature thermokarst lakes with water balances stabilized by the influence of regional runoff. Once such lakes are linked to rivers, they become influential as

headwater storage reservoirs and supply sources to downstream channels. While the characterization of lake-river interactions is beyond the scope of this analysis, it is evident that the thermokarst lake cycle is a key aspect of understanding environmental and ecological conditions in the SAYR, and water prediction and security in the Yellow River as a whole. Similar changes are occurring in the Tibetan headwaters of the Langcang (Mekong) and Chang-Jiang (Yangtze) Rivers which account for about 5% of global riverine discharge (Dai and Trenberth, 2002).

6. Conclusions

A water sampling program was carried out in 2014 and 2016 to collect and measure radioactive and stable isotopes of water (^{3}H, ^{2}H and ^{18}O) in lakes, wetlands, ground ice, supra-permafrost groundwater water and precipitation across the Source Area of the Yellow River, a region characterized by a mosaic of permafrost landscapes with active thermokarst lake development. The dataset was applied to evaluate lake water balances using stable isotope mass balance and a tritium gradient method to further understand the effects of permafrost degradation on lake water balances. The main conclusions of the research are as follows:

(1) A distinct increase in tritium content was found in thermokarst lakes under a gradient signifying progressively greater permafrost coverage, i.e. SFG < SDP < EDP, which were measured at 15.6 ± 0.7 T.U, 17.1 ± 2.0 T.U, and 20.4 ± 0.6 T.U, respectively. Higher tritium content is inferred to an indicator of source contributions from thawing permafrost. This is consistent with tritium values in ground ice that were found to be 21.2 ± 1.9 T.U.

(2) IMB revealed systematic gradients in water balance of lakes. E/I and P/I ratios increased along the gradient EDP < SDP < EDP < reference lakes, whereas WY and R/P were found to decrease. Reference lakes, together with SFG and SDP thermokarst lakes are defined as evaporation-dominated lakes ($E/I > 0.5$). Reference lakes were found to have negative water balances ($E/I > 1$), with direct precipitation on lake surfaces controlling the water balance and downstream flows. Slightly positive water balances in SFG thermokarst lakes ($0.6 < E/I < 1$) are attributed to watershed conditions which have limited hydrological connection to rivers. The limited role of permafrost drives a little more runoff to feed SDP thermokarst lakes within a positive balance. EDP thermokarst lakes have strongly positive water balances ($E/I < 0.3$) and receiving greatest runoff from permafrost meltwater.

(3) Using IMB models paired with the tritium decay gradients, an enhanced approach is presented for better understanding of short-term shifts in lake water balance. From 2014 to 2016, minor precipitation-related increases led to weak positive shifts of water balance in reference lakes and SFG lakes, while minor precipitation-related increases accompanied by significant permafrost meltwater contributions accounted for strong positive water balance shifts in EDP thermokarst lakes. Increasing contributions from thawing permafrost (estimated at 50 mm/year based on IMB) was found for EDP thermokarst lakes, which also was confirmed by higher tritium concentrations as well as tritium decay gradients. For SDP thermokarst lakes, negative shifts in water balances resulted from decrease in permafrost (estimated at close to 25 mm/year based on IMB). The approach serves as a useful framework for illustration and classification of thermokarst lake water balance, and emphasizes the value in tracing temporal isotopic shifts.

(4) Progressively, from EDP to SDP to SFG thermokarst areas, runoff conditions transitioned from high water yield dominated by permafrost thaw sources to low water yield dominated by precipitation sources. A conceptual model of thermokarst lake development and evolution was developed that provides context for the current spatial mosaic of permafrost landscapes observed across the SAYR. This provides a framework for predicting future changes in hydrology, and background for understanding headwater lakes that influence the future hydrology of the Yellow River.

Ongoing research is focused on analysis and interpretation of wider area surveys of thermokarst lakes in the SAYR including geochemical properties, as well as partitioning of source water contributions to the Yellow River using radon-222, tritium and stable isotopes to develop better understanding of hydrologic and biogeochemical processes affecting riverine source waters and their expected evolution due to continued permafrost degradation.

Acknowledgments

This research was supported by the State Key Program of National Natural Science Foundation of China (Grant No. 51539003), the Strategic Priority Research Program of Chinese Academy of Sciences (XDA2010010307), the Postgraduate Research & Practice Innovation Program of Jiangsu Province (Grant No. KYCX17_0418) and the Fundamental Research Funds for the Central Universities (Grant No. 2017B682X14; 2019B10114). The authors would like to especially acknowledge Paul Eby, InnoTech Alberta, for great support and rapid turnaround of isotopic analysis, and Qian Chen for sample collection and shipment. The authors are also grateful to three anonymous reviewers for their valuable suggestions.

References

Ala-Aho, P., Soulsby, C., Pokrovsky, O.S., Kirpotin, S.N., Karlsson, J., Serikova, S., ... Tetzlaff, D., 2018a. Permafrost and lakes control river isotope composition across a boreal Arctic transect in the Western Siberian lowlands. Environ. Res. Lett. 13 (3). https://doi.org/10.1088/1748-9326/aaa4fe.

Ala-Aho, P., Soulsby, C., Pokrovsky, O.S., Kirpotin, S.N., Karlsson, J., Serikova, S., ... Tetzlaff, D., 2018b. Using stable isotopes to assess surface water source dynamics and hydrological connectivity in a high-latitude wetland and permafrost influenced landscape. J. Hydrol. 556, 279–293. https://doi.org/10.1016/j.jhydrol.2017.11.024.

Anthony, K.M.W., Zimov, S.A., Grosse, G., Jones, M.C., Anthony, P.M., Iii, F.S.C., ... Frolking, S., 2014. A shift of thermokarst lakes from carbon sources to sinks during the Holocene epoch. Nature 511 (7510), 452–456. https://doi.org/10.1038/nature13560.

Arp, C.D., Jones, B.M., Urban, F.E., Grosse, G., 2011. Hydrogeomorphic processes of thermokarst lakes with grounded-ice and floating-ice regimes on the Arctic coastal plain, Alaska. Hydrol. Process. 25 (15), 2422–2438. https://doi.org/10.1002/hyp.8019.

Benettin, P., Penna, D., Kirchner, J.W., von Freyberg, J., Dawson, T.E., Frentress, J., Volkmann, T.H.M., 2018. Effects of climatic seasonality on the isotopic composition of evaporating soil waters. Hydrol. Earth Syst. Sci. 22 (5), 2881–2890. https://doi.org/10.5194/hess-22-2881-2018.

Biskop, S., Maussion, F., Krause, P., Fink, M., 2016. Differences in the water-balance components of four lakes in the southern-central Tibetan Plateau. Hydrol. Earth Syst. Sci. 20 (1), 209–225. https://doi.org/10.5194/hess-20-209-2016.

Boike, J., Grau, T., Heim, B., Günther, F., Langer, M., Muster, S., ... Lange, S., 2016. Satellite-derived changes in the permafrost landscape of central Yakutia, 2000–2011: wetting, drying, and fires. Glob. Planet. Chang. 139, 116–127. https://doi.org/10.1016/j.gloplacha.2016.01.001.

Bond, M.J., Carr, J., 2018. Permafrost thaw and implications for the fate and transport of tritium in the Canadian north. J. Environ. Radioact. 192 (March), 295–311. https://doi.org/10.1016/j.jenvrad.2018.07.006.

Burn, C.R., Michel, F.A., 1988. Evidence for recent temperature-induced water migration into permafrost from the tritium content of ground ice near Mayo, Yukon Territory, Canada. Can. J. Earth Sci. 25 (6), 909–915.

Carey, S.K., Pomeroy, J.W., 2009. Progress in Canadian snow and frozen ground hydrology, 2003–2007. Canadian Water Resources Journal 34 (2), 127–138.

Cartwright, I., Morgenstern, U., 2016. Using tritium to document the mean transit time and sources of water contributing to a chain-of-ponds river system: implications for resource protection. Appl. Geochem. 75, 9–19. https://doi.org/10.1016/j.apgeochem.2016.10.007.

Cartwright, I., Morgenstern, U., 2018. Using tritium and other geochemical tracers to address the "old water paradox" in headwater catchments. J. Hydrol. 563 (June), 13–21. https://doi.org/10.1016/j.jhydrol.2018.05.060.

Chen, M., Rowland, J.C., Wilson, C.J., Altmann, G.L., Brumby, S.P., 2014. Temporal and spatial pattern of thermokarst lake area changes at Yukon Flats, Alaska. Hydrol. Process. 28 (3), 837–852. https://doi.org/10.1002/hyp.9642.

Cheng, G., Jin, H., 2013. Permafrost and groundwater on the Qinghai-Tibet Plateau and in northeast China. Hydrogeol. J. 21 (1), 5–23. https://doi.org/10.1007/s10040-012-0927-2.

Cheng, G., Wu, T., 2007. Responses of permafrost to climate change and their environmental significance, Qinghai-Tibet Plateau. Journal of Geophysical Research: Earth Surface 112 (2), 1–10. https://doi.org/10.1029/2006JF000631.

Craig, H., Gordon, L.I., 1965. Deuterium and oxygen-18 in the ocean and marine atmosphere. In: Tongiorgi, E. (Ed.), Stable Isotopes in Oceanographic Studies and Paleotemperatures. Spoleto, Italy, pp. 9–130.

Dai, A., Trenberth, K.E., 2002. Estimates of freshwater discharge from continents: latitudinal and seasonal variations. J. Hydrometeorol. https://doi.org/10.1175/1525-7541(2002)003<0660:EOFDFC>2.0.CO;2.

Donchyts, G., Schellekens, J., Winsemius, H., Eisemann, E., van de Giesen, N., 2016. A 30 m resolution surfacewater mask including estimation of positional and thematic differences using Landsat 8, SRTM and OPenStreetMap: a case study in the Murray-Darling basin, Australia. Remote Sens. 8 (5). https://doi.org/10.3390/rs8050386.

Fedorov, A.N., Gavriliev, P.P., Konstantinov, P.Y., Hiyama, T., Iijima, Y., Iwahana, G., 2014. Estimating the water balance of a thermokarst lake in the middle of the Lena River basin, eastern Siberia. Ecohydrology 7 (2), 188–196. https://doi.org/10.1002/eco.1378.

Gao, Z., Niu, F., Lin, Z., Luo, J., Yin, G., Wang, Y., 2018. Evaluation of thermokarst lake water balance in the Qinghai–Tibet Plateau via isotope tracers. Sci. Total Environ. 636, 1–11. https://doi.org/10.1016/j.scitotenv.2018.04.103.

Gibson, J. J., & Edwards, T. W. D. (2002). Regional water balance trends and evaporation-transpiration partitioning from a stable isotope survey of lakes in northern Canada. Global Biogeochemical Cycles, 16(2), 10-1–10-14. doi:https://doi.org/10.1029/2001gb001839

Gibson, J.J., Birks, S.J., Yi, Y., Vitt, D., 2015. Runoff to boreal lakes linked to land cover, watershed morphology and permafrost melt: a 9-year isotope mass balance assessment. Hydrol. Process. 29, 3848–3861. https://doi.org/10.1002/hyp.10502.

Gibson, J.J., Birks, S.J., Yi, Y., 2016a. Stable isotope mass balance of lakes: a contemporary perspective. Quat. Sci. Rev. 131, 316–328. https://doi.org/10.1016/j.quascirev.2015.04.013.

Gibson, J.J., Birks, S.J., Yi, Y., 2016b. Higher tritium concentrations measured in permafrost thaw lakes in northern Alberta. Hydrol. Process. 30 (2), 245–249. https://doi.org/10.1002/hyp.10599.

Gibson, J.J., Birks, S.J., Yi, Y., Moncur, M.C., McEachern, P.M., 2016c. Stable isotope mass balance of fifty lakes in central Alberta: assessing the role of water balance parameters in determining trophic status and lake level. Journal of Hydrology: Regional Studies 6, 13–25. https://doi.org/10.1016/j.ejrh.2016.01.034.

Gibson, J.J., Birks, S.J., Jeffries, D., Yi, Y., 2017. Regional trends in evaporation loss and water yield based on stable isotope mass balance of lakes: the Ontario Precambrian Shield surveys. J. Hydrol. 544, 500–510. https://doi.org/10.1016/j.jhydrol.2016.11.016.

Gibson, J.J., Birks, S.J., Moncur, M., 2019. Mapping water yield distribution across the South Athabasca Oil Sands (SAOS) area: baseline surveys applying isotope mass balance of lakes. Journal of Hydrology: Regional Studies 21 (May 2018), 1–13. https://doi.org/10.1016/j.ejrh.2018.11.001.

Heslop, J.K., Anthony, K.W., Sepulveda-jauregui, A., Martínez, K.C., Bondurant, A., Grosse, G., Jones, M., 2016. Thermokarst-lake Methanogenesis along a Complete Talik (Thaw Bulb) Profile, (June), 2015–2016. https://doi.org/10.5194/bg-12-4317-2015.204.

Hinzman, L.D., Bettez, N.D., Bolton, W.R., Chapin, F.S., Dyurgerov, M.B., Fastie, C.L., ... Yoshikawa, K., 2005. Evidence and implications of recent climate change in Northern Alaska and other Arctic regions. Clim. Chang. 72 (3), 251–298. https://doi.org/10.1007/s10584-005-5352-2.

Horita, J., Wesolowski, D.J., 1994. Liquid-vapor fractionation of oxygen and hydrogen isotopes of water from the freezing to the critical temperature. Geochim. Cosmochim. Acta https://doi.org/10.1016/0016-7037(94)90096-5.

Horita, J., Rozanski, K., Cohen, S., 2008. Isotope effects in the evaporation of water: a status report of the Craig-Gordon model. Isot. Environ. Health Stud. 44 (1), 23–49. https://doi.org/10.1080/10256010801887174.

Jasechko, S., Gibson, J.J., Edwards, T.W.D., 2014. Stable isotope mass balance of the Laurentian Great Lakes. J. Great Lakes Res. https://doi.org/10.1016/j.jglr.2014.02.020.

Jin, H., He, R., Cheng, G., Wu, Q., Wang, S., Lü, L., Chang, X., 2009. Changes in frozen ground in the Source Area of the Yellow River on the Qinghai-Tibet plateau, China, and their eco-environmental impacts. Environ. Res. Lett. 4 (4). https://doi.org/10.1088/1748-9326/4/4/045206.

Kang, S., Yi, Y., Xu, Y., Xu, B., Zhang, Y., 2017. Water isotope framework for lake water balance monitoring and modelling in the Nam Co Basin, Tibetan Plateau. Journal of Hydrology: Regional Studies 12, 289–302. https://doi.org/10.1016/j.ejrh.2017.05.007 (August 2016).

Kokelj, S.V., Jorgenson, M.T., 2013. Advances in thermokarst research. Permafr. Periglac. Process. 24 (2), 108–119. https://doi.org/10.1002/ppp.1779.

Kokelj, S.V., Jenkins, R.E., Milburn, D., Burn, C.R., Snow, N., 2005. The influence of thermokarst disturbance on the water quality of small upland lakes, Mackenzie Delta region, Northwest Territories, Canada. Permafr. Periglac. Process. 16 (4), 343–353. https://doi.org/10.1002/ppp.536.

Lantz, T.C., Turner, K.W., 2015. Changes in lake area in response to thermokarst processes and climate in old crow flats, Yukon. Journal of Geophysical Research: Biogeosciences 120 (3), 513–524. https://doi.org/10.1002/2014JG002744.

Lewkowicz, A.G., Etzelmüller, B., Smith, S.L., 2011. Characteristics of discontinuous permafrost based on ground temperature measurements and electrical resistivity tomography, Southern Yukon, Canada. Permafrost Periglac. Process. 22, 320–342. https://doi.org/10.1002/ppp.703.

Li, X., Cheng, G., Jin, H., Kang, E., Che, T., Jin, R., ... Shen, Y., 2008. Cryospheric change in China. Glob. Planet. Chang. 62 (3–4), 210–218. https://doi.org/10.1016/j.gloplacha.2008.02.001.

Li, J., Sheng, Y., Wu, J., Feng, Z., Ning, Z., Hu, X., Zhang, X., 2016. Landform-related permafrost characteristics in the Source Area of the Yellow River, eastern Qinghai-Tibet Plateau. Geomorphology 269, 104–111. https://doi.org/10.1016/j.geomorph.2016.06.024.

Liljedahl, A.K., Boike, J., Daanen, R.P., Fedorov, A.N., Frost, G.V., Grosse, G., ... Zona, D., 2016. Pan-Arctic ice-wedge degradation in warming permafrost and its influence on tundra hydrology. Nat. Geosci. 9 (4), 312–318. https://doi.org/10.1038/ngeo2674.

Lin, Z., Niu, F., Xu, Z., Xu, J., Wang, P., 2010. Thermal regime of a thermokarst lake and its influence on permafrost, Beiluhe Basin, Qinghai-Tibet Plateau. Permafr. Periglac. Process. 21 (4), 315–324. https://doi.org/10.1002/ppp.692.

Lin, Z., Niu, F., Liu, H., Lu, J., 2011. Hydrothermal processes of Alpine Tundra Lakes, Beiluhe Basin, Qinghai-Tibet Plateau. Cold Reg. Sci. Technol. 65 (3), 446–455. https://doi.org/10.1016/j.coldregions.2010.10.013.

Luo, D., Jin, H., Jin, R., Lin, L., He, R., Chang, X., 2011. The extraction of watershed characteristics of the Source Area of Yellow River based on SRTM DEM with ArcGIS. 2011 International Conference on Remote Sensing, Environment and Transportation Engineering, RSETE 2011 - Proceedings, pp. 1799–1802 https://doi.org/10.1109/RSETE.2011.5964645.

Luo, D., Jin, H., Lü, L., Wu, Q., 2014a. Spatiotemporal characteristics of freezing and thawing of the active layer in the Source Areas of the Yellow River (SAYR). Chin. Sci. Bull. 59 (24), 3034–3045. https://doi.org/10.1007/s11434-014-0189-6.

Luo, D.L., HuiJun, J., Marchenko, S., Romanovsky, V., 2014b. Distribution and changes of active layer thickness (ALT) and soil temperature (TTOP) in the Source Area of the Yellow River using the GIPL model. Science China Earth Sciences 57 (8), 1834–1845. https://doi.org/10.1007/s11430-014-4852-1.

Luo, D., Jin, H., Marchenko, S.S., Romanovsky, V.E., 2018a. Difference between near-surface air, land surface and ground surface temperatures and their influences on the frozen ground on the Qinghai-Tibet Plateau. Geoderma 312 (March 2017), 74–85. https://doi.org/10.1016/j.geoderma.2017.09.037.

Luo, D.L., Jin, H.J., He, R.X., Wang, X.F., Muskett, R.R., Marchenko, S.S., Romanovsky, V.E., 2018b. Characteristics of water-heat exchanges and inconsistent surface temperature changes at an elevational permafrost site on the Qinghai-Tibet Plateau. Journal of Geophysical Research: Atmospheres 123 (18), 10,057–10,075. https://doi.org/10.1029/2018JD028298.

Luo, D., Jin, H., Jin, X., He, R., Li, X., Muskett, R.R., ... Romanovsky, V.E., 2018c. Elevation-dependent thermal regime and dynamics of frozen ground in the Bayan Har Mountains, northeastern Qinghai-Tibet Plateau, southwest China. Permafr. Periglac. Process. 29 (4), 257–270. https://doi.org/10.1002/ppp.1988.

Luo, D., Jin, H., Wu, Q., Bense, V.F., He, R., Ma, Q., ... Lü, L., 2018d. Thermal regime of warm-dry permafrost in relation to ground surface temperature in the Source Areas of the Yangtze and Yellow rivers on the Qinghai-Tibet Plateau, SW China. Sci. Total Environ. 618, 1033–1045. https://doi.org/10.1016/j.scitotenv.2017.09.083.

Ma, R., Sun, Z., Hu, Y., Chang, Q., Wang, S., Xing, W., Ge, M., 2017. Hydrological connectivity from glaciers to rivers in the Qinghai-Tibet Plateau: roles of suprapermafrost and subpermafrost groundwater. Hydrol. Earth Syst. Sci. 21 (9), 4803–4823. https://doi.org/10.5194/hess-21-4803-2017.

Macdonald, L.A., Turner, K.W., Balasubramaniam, A.M., Wolfe, B.B., Hall, R.I., Sweetman, J.N., 2012. Tracking hydrological responses of a thermokarst lake in the Old Crow Flats (Yukon Territory, Canada) to recent climate variability using aerial photographs and paleolimnological methods. Hydrol. Process. 26 (1), 117–129. https://doi.org/10.1002/hyp.8116.

MacDonald, L.A., Wolfe, B.B., Turner, K.W., Anderson, L., Arp, C.D., Birks, S.J., White, H., 2016. A synthesis of thermokarst lake water balance in high-latitude regions of North America from isotope tracers. Arctic Science 3 (2), 118–149. https://doi.org/10.1139/as-2016-0019.

Mao, D., Wang, Z., Yang, H., Li, H., Thompson, J.R., Li, L., ... Wu, J., 2018. Impacts of climate change on Tibetan lakes: patterns and processes. Remote Sens. 10 (3). https://doi.org/10.3390/rs10030358.

Narancic, B., Wolfe, B.B., Pienitz, R., Meyer, H., Lamhonwah, D., 2017. Landscape-gradient assessment of thermokarst lake hydrology using water isotope tracers. J. Hydrol. 545, 327–338. https://doi.org/10.1016/j.jhydrol.2016.11.028.

Niu, F., Lin, Z., Liu, H., Lu, J., 2011. Characteristics of thermokarst lakes and their influence on permafrost in Qinghai-Tibet Plateau. Geomorphology 132 (3–4), 222–233. https://doi.org/10.1016/j.geomorph.2011.05.011.

Pan, X., You, Y., Roth, K., Guo, L., Wang, X., Yu, Q., 2014. Mapping permafrost features that influence the hydrological processes of a Thermokarst Lake on the Qinghai-Tibet Plateau, China. Permafr. Periglac. Process. 25 (1), 60–68. https://doi.org/10.1002/ppp.1797.

Pan, X., Yu, Q., You, Y., Chun, K.P., Shi, X., Li, Y., 2017. Contribution of suprapermafrost discharge to thermokarst lake water balances on the northeastern Qinghai-Tibet Plateau. J. Hydrol. 555, 621–630. https://doi.org/10.1016/j.jhydrol.2017.10.046.

Ran, Y., Li, X., Cheng, G., 2017. Climate warming has led to the degradation of permafrost stability in the past half century over the Qinghai-Tibet Plateau. Cryosphere Discuss. 30 (July), 1–30. https://doi.org/10.5194/tc-2017-120.

Ren, W., Yao, T., Yang, X., Joswiak, D.R., 2013. Implications of variations in $\delta^{18}O$ and δD in precipitation at Madoi in the eastern Tibetan Plateau. Quat. Int. 313–314, 56–61. https://doi.org/10.1016/j.quaint.2013.05.026.

Roy-Leveillee, P., Burn, C.R., 2017. Near-shore talik development beneath shallow water in expanding thermokarst lakes, Old Crow Flats, Yukon. Journal of Geophysical Research: Earth Surface 122 (5), 1070–1089. https://doi.org/10.1002/2016JF004022.

Samalavičius, V., Mokrik, R., 2016. Tritium activity trend formation in groundwater of Quaternary aquifer system, south-eastern Lithuania. Geologija. Geografija 2 (4). https://doi.org/10.6001/geol-geogr.v2i4.3399.

Selroos, J.-O., Cheng, H., Vidstrand, P., Destouni, G., 2019. Permafrost thaw with thermokarst wetland-lake and societal-health risks: dependence on local soil conditions under large-scale warming. Water 11 (3), 574. https://doi.org/10.3390/w11030574.

Smith, L.C., 2005. Disappearing Arctic lakes. Science 308 (5727), 1429. https://doi.org/10.1126/science.1108142.

Tong, L., Xu, X., Fu, Y., Li, S., 2014. Wetland changes and their responses to climate change in the "Three-River Headwaters" region of China since the 1990s. Energies 7 (4), 2515–2534. https://doi.org/10.3390/en7042515.

Turner, K.W., Wolfe, B.B., Edwards, T.W.D., 2010. Characterizing the role of hydrological processes on lake water balances in the Old Crow Flats, Yukon Territory, Canada, using water isotope tracers. J. Hydrol. 386 (1–4), 103–117. https://doi.org/10.1016/j.jhydrol.2010.03.012.

Ulrich, M., Matthes, H., Schirrmeister, L., Schütze, J., Park, H., Iijima, Y., Fedorov, A.N., 2017. Differences in behavior and distribution of permafrost-related lakes in Central Yakutia and their response to climatic drivers. Water Resour. Res. 53 (2), 1167–1188. https://doi.org/10.1002/2016WR019267.

Wang, S., Sheng, Y., Li, J., Wu, J., Cao, W., Ma, S., 2018a. An estimation of ground ice volumes in permafrost layers in Northeastern Qinghai-Tibet Plateau, China. Chin. Geogr. Sci. 28 (1), 61–73. https://doi.org/10.1007/s11769-018-0932-z.

Wang, Y., Sun, Z., Sun, Y., 2018b. Effects of a thaw slump on active layer in permafrost regions with the comparison of effects of thermokarst lakes on the Qinghai–Tibet Plateau, China. Geoderma 314, 47–57. https://doi.org/10.1016/j.geoderma.2017.10.046 (October 2017).

Yang, M., Nelson, F.E., Shiklomanov, N.I., Guo, D., Wan, G., 2010. Permafrost degradation and its environmental effects on the Tibetan Plateau: a review of recent research. Earth Sci. Rev. 103 (1–2), 31–44. https://doi.org/10.1016/j.earscirev.2010.07.002.

Yang, Y., Wu, Q., Yun, H., Jin, H., Zhang, Z., 2016. Evaluation of the hydrological contributions of permafrost to the thermokarst lakes on the Qinghai-Tibet Plateau using stable isotopes. Glob. Planet. Chang. 140, 1–8. https://doi.org/10.1016/j.gloplacha.2016.03.006.

Yang, Y., Jiang, G., Zhang, P., 2017. Stable isotopic stratification and growth patterns of ground ice in permafrost on the Qinghai-Tibet Plateau, China. Permafr. Periglac. Process. 28 (1), 119–129. https://doi.org/10.1002/ppp.1892.

Yang, Y., Wu, Q., Jin, H., Wang, Q., Huang, Y., Luo, D., ... Jin, X., 2019. Delineating the hydrological processes and hydraulic connectivities under permafrost degradation on Northeastern Qinghai-Tibet Plateau, China. J. Hydrol. 569, 359–372. https://doi.org/10.1016/j.jhydrol.2018.11.068.

Yi, P., Wan, C., Jin, H., Luo, D., Yang, Y., Wang, Q., ... Aldahan, A., 2018a. Hydrological insights from hydrogen and oxygen isotopes in Source Area of the Yellow River, east-northern part of Qinghai–Tibet Plateau. J. Radioanal. Nucl. Chem. 317 (1), 131–144. https://doi.org/10.1007/s10967-018-5864-7.

Yi, P., Luo, H., Chen, L., Yu, Z., Jin, H., Chen, X., ... Hu, Q., 2018b. Evaluation of groundwater discharge into surface water by using Radon-222 in the Source Area of the Yellow River, Qinghai-Tibet Plateau. J. Environ. Radioact. 192 (November 2017), 257–266. https://doi.org/10.1016/j.jenvrad.2018.07.003.

Yi, P., Chen, X., Wang, Z., Aldahan, A., Hou, X., Yu, Z., 2018c. Iodine isotopes (129 I and I) in the hydrosphere of Qinghai-Tibet region. J. Environ. Radioact. 192 (December 2017), 86–94. https://doi.org/10.1016/j.jenvrad.2018.06.005.

Yoshikawa, K., Hinzman, L.D., 2003. Shrinking thermokarst ponds and groundwater dynamics in discontinuous permafrost near Council, Alaska. Permafr. Periglac. Process. 14 (2), 151–160. https://doi.org/10.1002/ppp.451.

Zheng, M.J., Wan, C.W., Du, M.D., Zhou, X.D., Yi, P., Aldahan, A., ... Gong, M., 2016. Application of Rn-222 isotope for the interaction between surface water and groundwater in the Source Area of the Yellow River. Hydrol. Res. 47 (6), 1253–1262. https://doi.org/10.2166/nh.2016.070.

Zheng, D., van der Velde, R., Su, Z., Wen, J., Wang, X., Yang, K., 2018. Impact of soil freeze-thaw mechanism on the runoff dynamics of two Tibetan rivers. J. Hydrol. 563 (June), 382–394. https://doi.org/10.1016/j.jhydrol.2018.06.024.